NATIONAL LIBRARY
OTTAWA

BIBLIOTHÈQUE NATIONALE
OTTAWA

CANADA

NAME OF AUTHOR......... *TILAK CHAND SHARMA*

TITLE OF THESIS... *An Investigation of Proximity Scattering in the* ^{7}Li *(d,nα)α and* ^{12}C *(d,np)* ^{12}C *Reactions*

UNIVERSITY.... *University of Alberta*

DEGREE FOR WHICH THESIS WAS PRESENTED..... *Ph. D*

YEAR THIS DEGREE GRANTED...... *Fall, 1972*

Permission is hereby granted to THE NATIONAL LIBRARY

OF CANADA to microfilm this thesis and to lend or sell copies

of the film.

The author reserves other publication rights, and

neither the thesis nor extensive extracts from it may be

printed or otherwise reproduced without the author's

written permission.

(Signed)...... *Tcsharma*

PERMANENT ADDRESS:

.. *Department of Physics*
.. *Laval University*
.. *Quebec., P. Q.*

DATED... *Oct. 27*.......19 *72*

THE UNIVERSITY OF ALBERTA

AN INVESTIGATION OF PROXIMITY SCATTERING

IN THE $^{7}Li(d,n\alpha)\alpha$ AND $^{12}C(d,np)^{12}C$ REACTIONS

by

TILAK CHAND SHARMA

A THESIS

SUBMITTED TO THE FACULTY OF GRADUATE STUDIES AND RESEARCH

IN PARTIAL FULFILMENT OF THE REQUIREMENTS FOR THE DEGREE

OF DOCTOR OF PHILOSOPHY

DEPARTMENT OF PHYSICS

EDMONTON, ALBERTA

FALL, 1972

THE UNIVERSITY OF ALBERTA

FACULTY OF GRADUATE STUDIES AND RESEARCH

The undersigned certify that they have read, and recommend to the Faculty of Graduate Studies and Research, for acceptance, a thesis entitled AN INVESTIGATION OF PROXIMITY SCATTERING IN THE $^7Li(d,n\alpha)\alpha$ AND $^{12}C(d,np)^{12}C$ REACTIONS   submitted by TILAK CHAND SHARMA   in partial fulfilment of the requirements for the degree of Doctor of Philosophy.

....
Supervisor

John M. Cameron

Douglas M. Sheppard

....

....

....

....
External Examiner

Date ....Oct. 24, 1972

ABSTRACT

The reaction $^7\text{Li}(d,n\alpha)\alpha$ was investigated in search of n-α proximity scattering at incident deuteron energies between 1.90 and 2.10 MeV. The previously reported effects attributed to rescattering following the formation of the resonance state at 16.63 MeV in $^8\text{Be}^*$ are not observed. Strong lines due to randoms were seen in the vicinity of the proximity scattering positions on the kinematic locus. Data were fitted well with the Breit-Wigner line shape plus a linear background. Conditions affecting the observation of such a rescattering are discussed.

Another reaction, $^{12}\text{C}(d,np)^{12}\text{C}$, was studied to look for conclusive evidence of the existence of proximity scattering between the first emitted neutron and a proton emitted from the decaying 3.5 MeV doublet in $^{13}\text{N}^*$. The data at incident deuteron energies E_d = 5.2, 5.4 and 5.75 MeV and E_d = 5.1, 5.26 and 5.4 MeV at two different sets of angles very clearly show the energy dependence of the proximity scattering. The data taken at 6.25 MeV, where rescattering is kinematically disallowed, show no enhancement, as expected. The data taken at E_d = 5.4 and angle setting $\theta_n = \theta_p = 0°$, $\phi_{np} = 35°$ also support the theoretical predictions made by Aitchison and Kacser. The data at E_d = 5.4 MeV do not give a good fit with a Breit-Wigner line shape plus n-p final state interaction and it has been concluded that the singlet and triplet states of the deuteron do not contribute

significantly to the observed rescattering enhancement.

In the ^{28}Si(d,np)^{28}Si reaction, no meaningful estimate of the contribution due to proximity scattering could be made because of the interfe r ing sequential decays.

ACKNOWLEDGEMENTS

TABLE OF CONTENTS

LIST OF FIGURES

CHAPTER 1

INTRODUCTION

The study of reactions with three or more particles in the final state, where there are two-body resonances accessible for one or more pairs of particles, are of fundamental importance to understand two-body forces in the presence or vicinity of a third particle. Such reactions have often been used to study particle-unstable states and can be described by mechanisms like quasi-free scattering, final state interactions and processes in which two of the three particles proceed as a resonance. These, along with simultaneous breakup which mainly gives the "background", will contribute to the yield at various places along the kinematic locus.

Under special circumstances, a particle emitted from a decaying intermediate resonance can rescatter with the third particle giving rise to an enhancement in the amplitude which may not be insignificant. Such a process was termed "Proximity Scattering" by Fox[1]), who considered, in a static limit, this second order effect in an effort to determine very short lifetimes of the states in the particle unstable resonances. Classically, two conditions must be satisfied for Proximity Scattering to take place, namely, the two rescattering particles should be emitted parallel to each other in the overall center-of-mass system and

the particle emitted later should have a greater velocity.

Following the methods applied in fundamental particle physics, a quantum mechanical treatment consisting of essentially the evaluation of Feynman diagrams has been applied by Schnitzer[2]) and Duck[3]). In particular, Aitchison and Kacser[4-8]) have given a complete theoretical formalism of rescattering. They derived the kinematic conditions for proximity scattering, both relativistically and in the non-relativistic limit. The detailed theoretical discussion is given in Chapter 2.

Since proximity scattering effects are the necessary consequence of the existing ideas about final state interaction theory, their verification (or lack of the same) is of basic importance. Predictions of observable rescattering in low energy nuclear reactions, soon stimulated experimental searches and rescattering enhancements have been reported in (d,np) reactions on ^{12}C[9]) and ^{40}Ca[10]). Both of these reactions were studied at a single incident energy only. Enhancement due to proximity scattering occurs at a low relative p-n energy very close to the energy of the $T = 1$ resonance in the n-p system. Although the formation of a singlet-deuteron is isospin-forbidden, it was suggested by Phillips[11,49]) that an admixture of $T = 0$ and $T = 1$ could also explain such bumps. Similar isospin mixing in the compound ^{14}N system has been used to explain the large cross sections observed for the $^{12}C(d,\alpha)^{10}B$ (1.74 MeV, $T = 1$) reaction at incident deuteron energies from 6 to 21 MeV.[50]).

More recently, the reaction $Li + d \rightarrow \alpha + \alpha + n$ has been

examined for evidence of rescattering between the neutron and an alpha particle emitted by the resonant ^{8}Be system. The first report, by Valkovic et al.[12], was of measurements made above 3.0 MeV bombarding energy in which they could find no evidence of a rescattering enhancement. Later results[13] for the same reaction at incident energies between 2.07 and 2.12 MeV did, however, appear to show a very clear effect. In view of the implications which strong rescattering effects in this reaction may have on many other analyses, further verification of n-α proximity scattering in the ^{7}Li + d[14] reaction was undertaken as a part of the present research. The present data have failed to confirm the rescattering enhancement reported by Thiévent et al.[13]. Sweeney et al.[15] also did not find any evidence of proximity scattering in this reaction. Further discussion continues in Chapter 4.

As the observance of proximity scattering has not yet been conclusively established, this was a strong motivation for the present work to further study the rescattering effects in the ^{12}C(d,np)^{12}C reaction at a number of bombarding energies under improved conditions. The present data show a clear energy dependence of proximity scattering in this reaction. Although the formation of isospin-forbidden singlet deuteron is highly improbable in this reaction, the data have been taken at the angle settings where the effect of final state interactions is considerably reduced. Also, some of the data were fitted with a Breit-Wigner line shape plus an admixture of singlet and triplet

states of the deuteron. The results of this work tend to support the belief that the final state interactions do not appreciably contribute to the observed proximity scattering enhancement. The results of the present work were submitted to the International Conference of Few Particle Problems in Nuclear Physics[57], UCLA, 1972; and have also been submitted to Nuclear Physics[58] for publication. Another report by Gemmeke et al.[59] presented to the above conference also supported our results. However, they put an upper limit of 15% on the singlet deuteron contribution to the observed enhancement, which is quite high as compared to the ~3% effect proposed on the basis of the present calculations. The detailed discussion of this reaction is given in section 4.2.

The experimental apparatus and procedures are described in Chapter 3. The singularities of the triangle graphs, as discussed by Aitchison and Kacser[8,16] also have applications to higher resonances in Elementary Particle Physics. Such possible applications are discussed in Chapter 5. Finally, Chapter 6 contains the conclusions of the present study.

CHAPTER 2

THEORY OF REACTION MECHANISMS

The present study is based upon Aitchison and Kacser's forma-
lism of "proximity scattering". Before a proper understanding of
this formulism can be attained, it is rather appropriate to
discuss various reaction mechanisms which are applied to explain,
in general, the reactions with three particles in the final state.
Such processes, as described below, can be represented by the
Feynman graphs shown in fig. 1.

2.1 Simultaneous Break-up

This process is shown in fig. 1a. Here the events are
randomly distributed in phase space without any preference for a
particular position on the three-body kinematic locus.

Time dependent perturbation theory gives the following tran-
sition probability for a given reaction [17]

$$W = \frac{2\pi}{\hbar} |M|^2 \rho_E \qquad [2.1]$$

where M is the matrix element of the perturbation Hamiltonian
between initial and final states and ρ_E is the density of
final states available to the reaction. If $|M|^2$ has no strong
energy dependence, then $|M|^2$ may be approximated with a constant
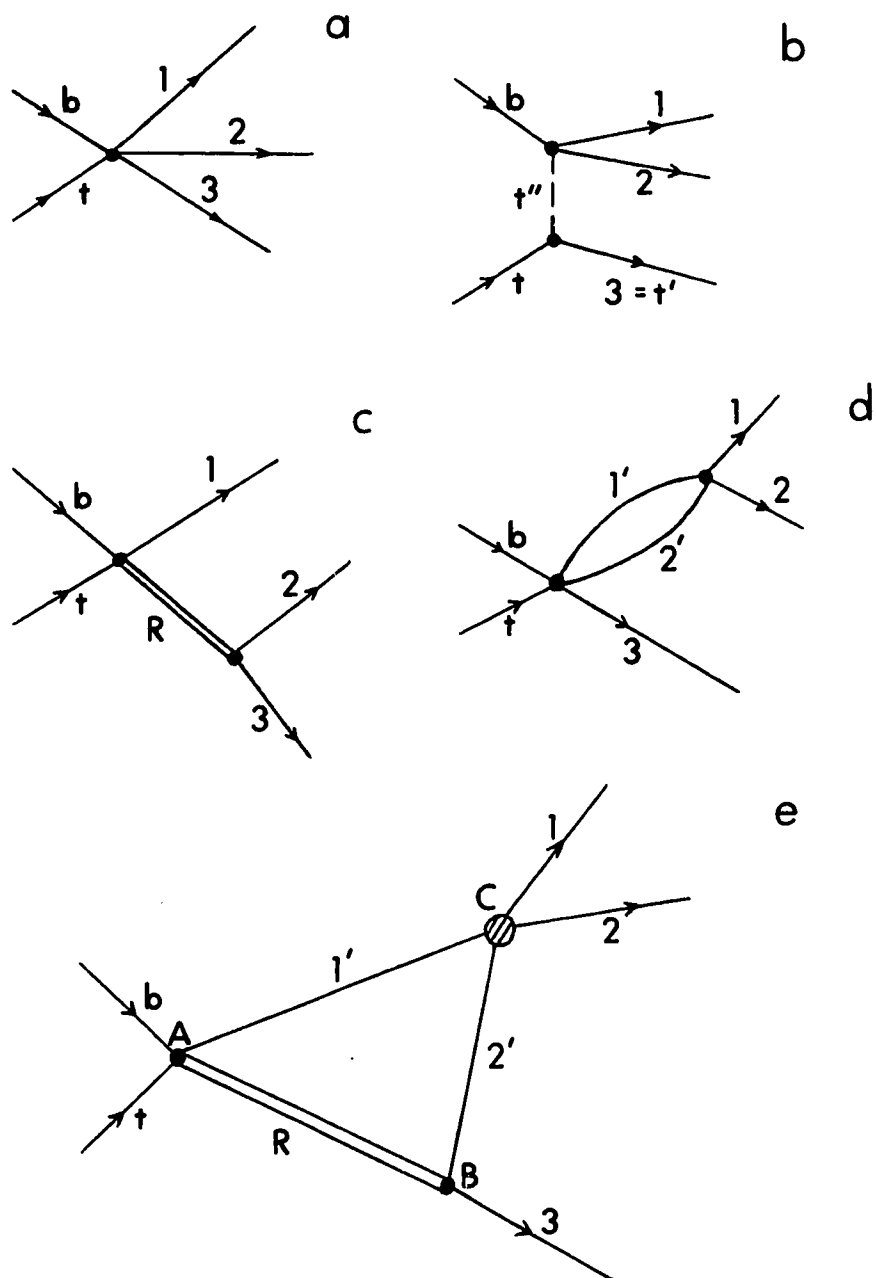
Figure 1   Feynman graphs for a) simultaneous breakup; b) quasi-free process; c) sequential decay; d) 'direct' interaction plus f.s.i.; and e) sequential decay plus proximity scattering.

and the cross section simply follows the phase-space. According to S-matrix theory, $|M|^2$ is a superposition of many Feynman diagrams. If there are no nearby poles, then no particular diagram will dominate and in the sum over many diagrams any rapid variation with energy will tend to cancel, leaving once again a constant matrix element. Thus the simultaneous break-up process is characterized by a constant matrix element in the transition probability. Experimentally, this normally represents the general background.

2.2 Quasifree Process

Cross-sections for reactions with two outgoing particles depend on two independent variables only, namely the centre-of-mass energy and angle; whereas in the three outgoing particles case it depends on three vector momenta with nine components, four of which can be eliminated by considerations of energy and momentum conservation. Thus we are left with five independent variables. One possible choice of these variables could be the total energy in the centre of mass system, three centre-of-mass angles specifying the directions of two outgoing particles with respect to each other and with respect to the beam axis, and the centre-of-mass energy of one outgoing particle. However, it is advantageous to choose as independent kinematic variables the squares of the velocity differences $(\vec{v}_i - \vec{v}_j)^2$, which are both scalars and Galilean invariants and may thus be evaluated in any inertial frame of reference.

When i is an incoming particle and j an outgoing one, $m_i m_j (\vec{v}_i - \vec{v}_j)^2$ is within a constant mass term, equal to the square of the four-momentum transfer between particles i and j. Experimental knowledge reveals that in three-particle reactions if the incoming particle interacts with only one constituent of the other incoming particle, the intensity maximum may be observed at a particular value of a momentum transfer variable. This is most likely to happen when the constituent is light and weakly bound so that it is often encountered far out in the periphery of the nucleus or some nuclear core. Such a process is, therefore, called peripheral or quasifree.

When the initial relative energy of the projectile and target is large compared to the binding energy of some of their constituents, one may neglect the binding energy and treat the collision as quasifree. Looking at fig. 1b, which is a Feynman diagram for a quasifree process, the most general peripheral process can be described as a two-body collision of the projectile b with either the particle t" or the core t' such that the target is broken up. The struck constituent of the target interacts with the projectile to give the final particles 1 and 2, while the other constituent of the target is only slightly affected and thus emerges with small laboratory momentum as particle 3.

Such a process can be computed in the PWBA, where all particles are treated as free, except for the initial bound state b , which is described by a bound state wave function $\psi(\vec{r}_{t'} - \vec{r}_{t''})$. The

matrix element will be the product of two factors, one for each vertex. The lower vertex yields a form factor which is the Fourier transform of the initial bound state wave function, the momentum variable of this transform being the momentum transferred during the collision to t'. In the laboratory system where the initial velocity of t is zero, this momentum transfer is just $\vec{p}_3$ and the Fourier transform is

$$\psi(\vec{p}_3) = \int \exp(i\vec{p}_3 \cdot \vec{x}) \, \psi(\vec{x}) \, d\vec{x} \qquad [2.2]$$

The upper vertex yields the Born-Approximation amplitude for the reaction b + t" → 1 + 2. One may improve upon this calculation by inserting at this point the exact two-body collision amplitude instead of the Born amplitude. For practical calculations, it is, at this stage, simplest to forget about the binding of the struck particle and assume a two-body collision. This procedure is known as the "Peripheral Model" or the "Impulse Approximation" (Refs. [18],[19]). Zupančič[33] has obtained the following expression for the three-body cross section:

$$d^4\sigma = k \left(\frac{T_i^{cm}}{T_f^{cm}} \right)^{\frac{1}{2}} \left(\frac{d\sigma}{d\Omega} \right)_{cm} |\psi(\vec{p}_3)|^2 \times \text{phase-space factor}$$

$$[2.3]$$

where   k   is a constant.

     $d^4\sigma$ is the three-particle cross-section for outgoing particles ending in an infinitesimal region of

final momentum-space .

$$\left(\frac{d\sigma}{d\Omega}\right)_{cm} = \left(\frac{d\sigma}{d\Omega}\right)_{\theta_{cm}}$$ is the two-body differential cross-section

for the reaction $b + t'' \rightarrow 1 + 2$ as measured in the

two-body centre-of-mass system at a relative final

energy T_f^{cm}.

$$T_f^{cm} = [m_1 m_2 / 2(m_1 + m_2)] (\vec{v}_1 - \vec{v}_2)^2$$

$$\theta_{cm} = arccos \frac{(\vec{v}_b - \vec{v}_{t''}) \cdot (\vec{v}_1 - \vec{v}_2)}{|\vec{v}_b - \vec{v}_{t''}| |\vec{v}_1 - \vec{v}_2|}$$

and

$$T_i^{cm} = [m_b m_{t''} / 2(m_b + m_{t''})] (\vec{v}_b - \vec{v}_{t''})^2$$

The velocity $v_{t''}$ may be calculated from momentum conservation in

the lower vertex. The term $|\psi(\vec{p}_3)|^2$ in expression (2.3) gives the

gross behaviour of the three-particle cross-section for a peripheral

process, because this represents the probability distribution for

the momentum of particle t" in the target. In this model the

reaction proceeds as if it were a free two-body reaction but with

an initial velocity spread of the struck particles t".

The various limitations in applying the peripheral model to

three-particle final state reactions can be enumerated as: the

requirement that the incident energy be large compared to the

reduced binding energy of particle t" in the target, the condition

that the final velocity of particles 1 and 2 relative to t' be

sufficiently large so that they escape quickly from the sphere of

influence of t', and finally, that the incident particle b should not interact strongly with the core t' while striking the particle t".

In nuclear physics, this model can be applied to knockout reactions at energies above 100 MeV, by using the extrapolation procedure suggested by Chew and Low[20]) which overcomes many of the limitations of this model. Eq. (2.3) enables us to extract rather important two-body parameters from three-body cross sections that are otherwise inaccessible; e.g., $d\sigma/d\Omega$ for a two-body collision for the cases where t" is unstable and hence the conventional methods cannot be applied. Another useful quantity is the form factor $|\psi(\vec{p}_3)|^2$. In complicated composite systems, such as most nuclei but the lightest ones, $\psi(\vec{x})$ represents only that component of the total wave function which describes the virtual disintegration of the target t into particle t" and core t'. When the target does not behave as a loosely bound system of t' and t", $|\psi(\vec{p}_3)|^2$ and the corresponding enhancement of the three-particle cross-section is small, which gives important clues to our understanding of the nuclear wave function. Finally, studies of the binding energies of nucleons in different shells of nuclei are made possible by the quasi-free scattering process which knocks a nucleon out from the interior of the nucleus without giving the latter time to rearrange itself.

2.3 Sequential Decay

In the case of short-lived systems (systems with a lifetime comparable to the transit time of a low energy proton through a light nucleus) the term "sequential" implies that the distribution of events within the available phase-space is not random, but is modulated by the interactions among pairs of components of the final state. Consider the reaction:

$$b + t \rightarrow 1 + (2+3)$$
$$ \big\lfloor\!\!\rightarrow 2 + 3 \qquad\qquad [2.4]$$
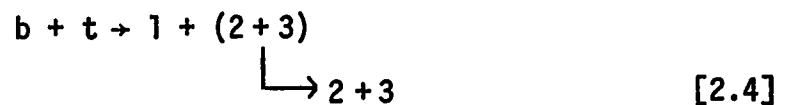
where b and t are incident and target nuclei respectively, and 1, 2 and 3 are the particles in the final state.

Here the system (2 +3) is short lived. The reaction will, in general, proceed in such a manner that the system (2 +3) is left with a relative internal energy E_{23} which corresponds to a resonance in the amplitude for the scattering of 2 on 3. In other words, the sequential processes are characterized by an intensity maximum in the three-particle cross-section at a particular value of the internal energy variable which, in this case, will be the relative energy E_{23}:

$$E_{23} = [m_2 m_3 / 2(m_2 + m_3)] (\vec{v}_2 - \vec{v}_3)^2 \qquad\qquad [2.5]$$

If (2 +3) is a sufficiently long-lived system such that the probability of decay during the time that 1 and (2 +3) are separated by distance comparable to the range of nuclear forces is small, then the decay of the system (2 +3) will essentially be independent of 1 and the decay process of the recoiling system will depend entirely on the properties of the intermediate state; i.e. the angular distribution of the decay will be determined by the angular momentum of the state and the branching ratio for the decay to the various internal states of 2 and 3 will depend upon the internal structure of the recoiling system.

The formation and subsequent decay of a meta-stable system in nuclear physics can be explained analogously to the excitation of an atomic or molecular state by electron impact and its subsequent decay by the emission of a photon[26]). The following expression[20]) can be applied very well for the reaction given in eq. (2.4):

$$d^2\sigma_1 \;=\; \frac{\Gamma_{fx}}{\Gamma}\;\frac{\Gamma}{2\pi}\;\frac{dE_{23}}{\left(E_{23}-\Delta E\right)^2 + \dfrac{\Gamma^2}{4}}\; d\sigma_0 \qquad\qquad [2.6]$$

where the (2 +3) system decays from the state x to the final state f and ΔE is the energy difference between the centre of the excited state x and the final state f.

Also, $\dfrac{\Gamma_{fx}}{\Gamma}$ is the relative probability for the decay of the excited state x to the final state f;

E_{23} is the relative energy of the (2 +3) system;

Γ is the total width of the resonance (2 + 3) which is

assumed to be small;

and $d\sigma_0$ is the differential cross section for the process

b + t → 1 + (2 + 3), ignoring the subsequent break-up

of (2 + 3).

Equation (2.6) shows the dependence of the three-body cross

section on the relative energy E_{23} of 2 and 3 as revealed by the

energy spectrum of 1. However, particle decaying states are usually a

few orders of magnitude wider as compared to the gamma decaying

states; this may give rise to important differences in shape and

position of the resonance as observed under different conditions.

This is due to the energy dependence of the widths Γ and Γ_{fx}

which are in general not negligible in the case of nuclear

reactions. Since a width Γ is a product of an energy-independent

reduced width and a penetration factor, such effects are particu-

larly noticeable when penetration factors are fast varying. For

example, in the Coulomb penetration factors at low energies which

generally are increasing functions of energy, a two-body resonance

would produce a peak in the three-particle cross section at a

value of E_{23}, which is somewhat lower than the corresponding peak

energy of the isolated two-body cross section. Another important

point to notice is that for two-body elastic scattering, the

potential scattering amplitude must be added to the resonance

scattering amplitude. Especially when the Coulomb scattering is

important, the interference term may violently change the shape of

the two-body elastic scattering cross-section in the resonance region. A classical example of the use of this theory is the deduction by Werntz[21]) of the existence, energy, and spin of the first excited state of the α-particle from the t(d,pn)t experiment of Lefevre et al.[22]). In this case the resonance in the t-p system was deduced from the neutron energy spectrum. The initial direct process is a (d,n) rearrangement collision leaving the proton and triton in a resonant state. The wave function of the resonant t-p system was deduced from the neutron energy spectrum. The wave function of the resonant t-p system differs from a bound state wave function in that it has different boundary conditions. Asymptotically, it is the direct product of a triton wave function with a proton wave function, which has plane waves superimposed on ingoing spherical waves. One of the partial waves in this wave funciton is assumed to be resonant, and the resonance parameters are determined by curve fitting.

Existing experimental evidence has shown that most of the multibody final state nuclear reactions induced by low energy projectiles proceed to the final state by various sequential processes[23]).

Two nucleon systems, namely, pn, nn and pp belong to an exceptional case, where the two-body cross-section does not

exhibit a proper resonance and yet the three-particle reaction may be considered to be approximately sequential, when the intermediate system is in a relative s-state at a very low energy. Their decay is certainly not exponential, thus they do not possess a uniquely defined lifetime. However, one may well consider the average time they spend together, as a function of their relative energy. Since their relative position is uncertain within their relative wavelength, this time may be defined as:

$$\tau = v^{-1} (r + \frac{1}{k} + \frac{d\delta}{dk})$$ [2.7]

where v and k are the relative velocity and wave number, respectively, r is the range of the nuclear interaction, and δ is the nuclear phase shift. In the effective range approximation, δ is given by $k \cot \delta = -\frac{1}{a} + \frac{1}{2} r_0 k^2$. Thus one may compute the average lifetime of two nucleon systems. One finds that in the interesting low energy region, it is indeed long compared to 10^{-22} sec. (the time taken by 10 MeV protons to traverse an ^{16}O nuclear radius) and in general is also long compared to the time spent by the third particle in traversing the distance $r + \frac{1}{k}$. In this sense, one may consider reactions involving the formation of the two-nucleon system at a low relative energy, as quasi-sequential. In such cases it is customary to speak of final state interactions rather than intermediate systems.

2.4 Final State Interactions

Final state interactions (f.s.i.) are important since they may modify the observed energy spectra and angular distributions without playing any part in the primary production mechanism. In order to have a calculable effect for the f.s.i., three general conditions must be satisfied, namely, i) the primary reaction should be a short range interaction, ii) the f.s.i. is to be considered for low relative energies of the particles involved, and iii) it must be strong and attractive.

The existing experimental evidence shows that the cross section for three-body interactions depends on the relative energies of the pairs of interacting particles and appears to be independent of the momentum transfer type variables which characterize the production amplitude. Such a dependence allows us to deal separately with the primary interaction (i.e. the production process) and the f.s.i. between the pairs of interacting particles, which is quite useful in that the two processes can be studied separately by varying the momentum transfer variable and relative energy.

The theory of final state interactions depends on the assumption of successive independent interactions. This assumption is valid if the lifetime of the final state two-particle system is sufficiently long for its decay not to be influenced by the presence of the third particle. In reactions involving nucleons, the $^1s_0$ interaction of two nucleons can produce a virtual state which approximately satisfies

this requirement. Such a state is not a Breit-Wigner type of resonance and is not an exponentially decaying state. For example, in a p-n system, the $^1s_0$ phase shift has a rapid increase at about 70 keV p-n relative energy. A rapidly increasing phase shift may be interpreted as a time delay[26]) and the lifetime may be so defined. This leads to a pole in the scattering amplitude for such states, which has the form

$$\frac{1}{K_{rel} + i \left(\frac{1}{a}\right)}$$

where K_{rel} is the relative momentum of the two interacting nucleons and a is the scattering length of the effective range theory[27]). Since this expression has a maximum at zero relative energy, the interaction is sometimes referred to as a zero-energy resonance.

The earlier remark about f.s.i. being strong and attractive is supported by a time-reversal argument introduced by Watson[28]) who proposed that a f.s.i. causes the three-body cross section to have the same energy dependence as the elastic scattering cross section of the two relevant particles. He considered the reaction to proceed backwards in time. If two of the particles interact and stick together for awhile, then there is a relatively higher probability for the three particles to be found in the primary interaction volume and undergo the inverse primary reaction.

The probability that the two particles interact is given by their differential cross section; by detailed balancing, the three body reaction cross section is just proportional to this cross section times a production amplitude and phase-space factors, i.e.

$$d\sigma \simeq d^3q \; \sigma_q^0 \; \text{times other factors} \qquad [2.8]$$

where q is the small relative momentum of the two particles and σ_q^0 is their scattering cross section for the relative momentum q. d^3q is a factor in the volume of phase-space into which the reaction proceeds. q is supposed to be small enough so that σ_q^0 arises only from s-wave scattering. For $q \simeq 0$, the q dependence of the "other factors" in eq. (2.8) can be neglected, leaving only that of

$$d^3q \; \sigma_q^0 \simeq dq \sin^2 \delta_q \qquad [2.9]$$

where δ_q is the s-wave phase-shift for the scattering at relative momentum q. When $\sin^2 \delta_q$ becomes of the order of unity (which occurs for values of q such that $\frac{\hbar}{q}$ is still large compared to the range of the primary interaction) a strong correlation in the emission of the interacting particles will result which can be described by eq. (2.9). This equation then gives a means of measuring δ_ℓ from an observation of the reaction cross section.

A general form of the cross section enhancement factor may be

derived by means of the factored wave function method[29]). The

transition matrix element can be written as

$$T_{ba} = <\psi_b |T| \psi_a> ;$$

<div align="right">[2.10]</div>

Instead of the usual final state consisting of plane waves

for the three particles, a state consisting of plane waves for

the non-interacting particle and for the c.m. of the remaining

pair may be substituted; the relative motion of the interacting

pair (labelled 1 and 2) is then described by the Schrödinger

wave function ψ calculated with the potential U for relative

momentum q and separation $\vec{r} = \vec{r}_1 - \vec{r}_2$. This implies the

substitution

$$\psi_b = \chi(\vec{r}_1) \chi(\vec{r}_2) \chi(\vec{r}_3) \rightarrow \chi(\vec{r}_3) \chi(\vec{r}_1 + \vec{r}_2) \psi(q, \vec{r}_1 - \vec{r}_2)$$

<div align="right">[2.11]</div>

where

$$(- \frac{d^2}{dr^2} + U) \psi = q^2 \psi$$

<div align="right">[2.11a]</div>

Since $<\psi_b |T| \psi_a>$ is only large inside the production region,

$\psi(q,0)$ may be factored out;

$$<\psi_b |T| \psi_a> = \psi(q,0) <\psi_b |T^{(0)}| \psi_a>$$

<div align="right">[2.12]</div>

where $T^{(0)}$ is the production matrix element. Thus $|\psi(q,0)|^2$ is

the enhancement factor. This result can be formally obtained using the Lippmann-Schwinger formalism as described by Gillespie[30]). Watson[28]) used his own model to derive an expression for the enhancement factor.

Fermi[31]) first suggested a normalization to the enhancement factor by taking the ratio of the wave function $\psi(q,0)$ to the wave function corresponding to a zero phase-shift evaluated at a radius equal to the range of the interaction. This result can be explicitly derived in potential theory by means of the Jost function formalism[32]).

In Watson's model, $\psi(q)$ is assumed to have the same momentum dependence as its asymptotic form. The asymptotic wave function for s-wave continuum states is given by

$$\psi(k,r) = \frac{e^{-i\delta} \sin(kr+\delta)}{kr} \qquad [2.13]$$

and in the effective range approximation the phase shift δ is given by

$$k \cot \delta = -\frac{1}{a} + \frac{1}{2} r_0 k^2 \qquad [2.14]$$

where r_0 is the effective range; thus at low energies

$$\psi(k,r) \simeq \frac{e^{-i\delta} \sin\delta}{kr} \left(1 + \frac{r}{a}\right) \qquad [2.15]$$

for $k\, r_0 \ll 1$. The first term of this expansion is the scattering amplitude which is the cross section enhancement factor.

Following the Fermi rule for normalization:

$$\frac{\psi(k,r_0)}{\psi^{(0)}(k,r_0)} = \frac{e^{i\delta}\,\sin\delta\,(1+\frac{r_0}{a})}{\sin k\, r_0} \qquad [2.16]$$

Solving eq. (2.14) for δ one gets

$$\frac{\psi(k,r_0)}{\psi^{(0)}(k,r_0)} = \frac{e^{i\delta}(\frac{1}{r_0}-\frac{1}{a}+\frac{1}{2}\,r_0\,k^2)}{(k^2+(\frac{1}{a}-\frac{1}{2}\,r_0\,k^2)^2)^{\frac{1}{2}}} \qquad [2.17]$$

and squaring, we get the enhancement factor:

$$E = \frac{(\frac{1}{r_0}-\frac{1}{a}+\frac{1}{2}\,r_0\,k^2)^2}{k^2+(\frac{1}{a}-\frac{1}{2}\,r_0\,k^2)^2} \qquad [2.18]$$

For the p-p interaction[33,34] Coulomb repulsion has to be included to give the corresponding expression for the enhancement factor:

$$E_{pp} = \frac{(\frac{1}{r_0}-\frac{1}{a}+\frac{1}{2}\,r_0\,k^2-\frac{1}{\rho}\,h(\eta))^2}{c^2k^2+\frac{1}{c^2}(\frac{1}{a}-\frac{1}{2}\,r_0\,k^2+\frac{1}{\rho}\,h(\eta))^2} \qquad [2.19]$$

where $\quad c^2 = \dfrac{2\pi\eta}{e^{2\pi\eta}-1}\quad,\quad \eta = \dfrac{e^2}{\hbar v}$

$\rho = \dfrac{\hbar^2}{me^2}$ and $h(\eta)$ is a function evaluated by Jackson and Blatt[35]), m and e are the mass and charge of the proton, and v is the relative velocity of the p-p system.

Gillespie and others[36]) have reviewed a more formal treatment of f.s.i. theory. They show that for s-wave interactions

$$\psi(k,r) = \frac{\frac{1}{2}i}{f(-k)} [f(-k)e^{-ikr} - f(k)e^{ikr}] \qquad [2.20]$$

where $f(k)$ may be related to the S-matrix by $S(k) = \dfrac{-f(k)}{f^*(k)}$. A consideration of the boundary condition at large r then yields the enhancement factor

$$E = \left| \frac{\psi(k,r)}{\psi^{(0)}(k,r)} \right|^2 = \lim_{r \to 0} \frac{1}{|f(-k)|^2} \qquad [2.21]$$

Jost and Kohn[37]) have shown $f(-k)$ to be identical to the Fredholm determinant, which can be shown to be the D-function of the dispersion relations. Jost function formalism gives

$$\frac{1}{f(-k)} = \frac{k + i\alpha}{k + i\beta} \qquad [2.22]$$

where $\quad \dfrac{1}{2} r_0 (\alpha - \beta) = 1$

$\quad\quad\quad \dfrac{1}{2} r_0 \alpha\beta = \dfrac{1}{a}$

and $\quad k \cot \delta = -\dfrac{1}{a} + \dfrac{1}{2} r_0 k^2$.

The enhancement factor becomes

$$E = \left| \frac{1}{f(-k)} \right|^2 = \frac{[\frac{r_0}{2}(\alpha^2 + k^2)]^2}{k^2 + (\frac{1}{a} - \frac{1}{2} r_\alpha k^2)^2} \qquad [2.23]$$

which is identical to the expression (2.18), since

$$\alpha^2 \simeq (- \frac{1}{a} + \frac{1}{r_0}) \frac{2}{r_0}. \qquad [2.24]$$

The parameters a and r_0 are shown in this theory to arise from the use of the pole approximation in S-matrix theory. This yields an effective-range type parametrization and enables the enhancement factor to be approximated by the scattering amplitude.

A more general but exact treatment of f.s.i. has been given by Phillips, Griffy and Biedenharn[38]), using the generalized density-of-states function in the continuum. The reaction

$$a + A \to D^* \to b + B \qquad [2.25]$$

for sharp states B has been treated by the perturbation theory to yield the differential cross section for particle b,

$$\frac{d^2\sigma}{dE_b\, d\omega_b} = \frac{\mu_a\, \mu_b\, k_b}{4\pi^2\, \hbar^2\, k_a} \left| \langle B + b,\, E_b | H' | A + a,\, E_a \rangle \right|^2 \rho(E_B) \qquad [2.26]$$

where H' is the interaction Hamiltonian for eq. (2.25) and $|A + a,\, E_a\rangle$ and $|B + b,\, E_b\rangle$ represent the initial and final state vectors, respectively. k_a and k_b are initial and final

wave numbers, whereas, $\rho(E_B)$ is the generalized density-of-states function for sharp states B with eigenenergies E_n:

$$\rho(E_B) = \sum_n \delta(E - E_n)$$
[2.27]

If B is not a sharp state, but is a virtual or resonant state which decays further into two particles

$$B \to c + C$$
[2.28]

then the generalized density of states (eq. 2.26) for sharp states must be replaced by that for a semistable particle B. The generalized density of states function enables the scattering to be described in terms of the experimental phase shifts for scattering of the final state particles and no knowledge of the inter-particle interaction is required. In the resonant scattering approximation, the generalized density-of-states method gives the same amplitude as obtained using the resonant-pole intermediate state method, provided the sum is taken over all possible alternate semi-stable states of B.

2.5 Rescattering or Proximity Scattering Process

At low energies, the quasifree process shown in fig. 1b is not of importance. The processes represented in figs. 1a, 1c and 1d combined together, essentially constitute the Watson-Migdal model[24,28]. Fig. 1c represents the sequential decay in which

particle 1 and (2+3) as a resonance R, are emitted when the incident particle b strikes the target nucleus t . R then decays after a time delay characteristic of the width of this resonance into particles 2 and 3.

Subsequent to this reaction, fig. 1e corresponds to a second order refinement or correction where particles 2 and 1 can further rescatter, in general elastically, giving rise to an enhancement in the cross section. This is a perfectly valid physical process and a complete mathematical formulation has been given by Aitchison and Kacser[+]. An outline of this formalism is described below.

a) Kinematics:

Let us consider the reaction

$$b + t \rightarrow w \rightarrow 1 + 2 + 3 \qquad [2.29]$$

where the particles have masses m_b, m_t, m_1, m_2 and m_3; and w is the total invariant mass in the over-all centre-of-mass system. Ignoring the momentum transfer type variables, the usual relativistic variables used to describe the three-body final state are given by

$$s = (E_1 + E_2)^2 - (\vec{p}_1 + \vec{p}_2)^2$$

$$= m_1^2 + m_2^2 + 2 (E_1 E_2 - \vec{p}_1 \cdot \vec{p}_2) \qquad [2.30]$$

and similarly for t and u, so that

$$s + t + u = W^2 + m_1{}^2 + m_2{}^2 + m_3{}^2 \qquad [2.31]$$

where $c = 1$.

In order to study the allowed physical region for fixed W^2, with $W > m_1 + m_2 + m_3$, consider the (12) c.m. frame, in which the initial system $(b + t) = W$ has three-momentum $\vec{p}$, as has particle 3, while particles 1 and 2 have momenta $\vec{q}$ and $-\vec{q}$, respectively. Then in the non-relativistic (N.R.) limit

$$p^2 \rightarrow 2\, m_3 \, m_{123} \, (Q - E_{12}) \, / \, m_{12} \qquad [2.32]$$

$$q^2 \rightarrow 2\, \mu_{12} \, E_{12} \qquad [2.33]$$

$$t \rightarrow W^2 + m_1{}^2 - 2E_W \, E_1 + 2\, pq \, \cos \theta \qquad [2.34]$$

where

$$Q = (W - m_1 - m_2 - m_3)\, c^2 \qquad [2.35]$$

$$m_{123} = m_1 + m_2 + m_3$$

$$m_{ij} = m_i + m_j$$

and

$$\mu_{ij} = \frac{m_i m_j}{m_i + m_j}$$

from (2.32) and (2.33), we get a relation between p and q :

$$p^2 \rightarrow \frac{2\,m_2 m_{123}}{m_{12}} \left(Q - \frac{q^2}{2\mu_{12}}\right) \qquad [2.36]$$

The boundary of the allowed region occurs when all three particles have collinear momenta in the (12) c.m. system, or equivalently, in the overall c.m. system. The equation of the boundary curve, in the N.R. limit is

$$[m_{23}\, m_{12}\, (E_{12} + E_{23}) - Q\, m_{123}\, m_2]^2$$

$$- 4\, E_{23}\, E_{12}\, m_{23}\, m_{12}\, m_3\, m_1 \rightarrow 0 \qquad [2.37]$$

Solving for E_{12} in terms of E_{23}

$$E_{12} \rightarrow \frac{1}{2}\frac{\mu_{12}\, m_3}{m_{23}} \left[\left(\frac{2E_{23}}{m_2}\right)^{\frac{1}{2}} \pm \left(\frac{2(Q-E_{23})\, m_{123}}{m_1 m_3}\right)^{\frac{1}{2}} \right]^2 \qquad [2.38]$$

In order to derive the kinematics of the "Rescattering Conditions", consider the intermediate process $R + 1' \rightarrow 3 + 2' + 1'$ in fig. 1e. In the over-all c.m. system, if $1'2'$ rescattering is to occur, the velocity $\vec{v}'_2$ of 2 must be parallel to $\vec{v}'_1$, and also $v'_2 > v'_1$. But if $\vec{v}'_2$ is parallel to $\vec{v}'_1$, it follows that $\vec{p}_1'$, $\vec{p}_2'$ and $\vec{p}_3$ are all collinear. This implies that a necessary condition for the rescattering is that $\vec{p}_1'$, $\vec{p}_2'$ and $\vec{p}_3$ correspond to a point on the boundary of the phase space.

In the N.R. limit, this condition can be expressed in terms

of $E_{1'2'}$ and $E_{2'3}$. Defining $Q_{R\to23} = (m_R - m_2 - m_3) c^2$, $E_{2'3}$ will be given by $E_{2'3} \to Q_{R\to23}$. Then using eq. (2.38),

$$E_{1'2'} = \frac{1}{2} \mu_{12} \left[(\frac{2m_3 \, Q_{R\to23}}{m_2 \, m_{23}})^{\frac{1}{2}} \pm (\frac{2(Q - Q_{R\to23})m_{123}}{m_{23} \, m_1})^{\frac{1}{2}} \right]^2 \qquad [2.39]$$

Equation (2.39) can also be derived more directly[12]. Each term has a physical significance: namely, the square roots are precisely the velocities of particles 2 and 1, respectively, before rescattering, in the rest frame of (23) resonance. This equation is a necessary condition, in that it is needed to ensure that v_2' and v_1' are collinear. In order that they will also be parallel, as opposed to antiparallel, only the smaller of the two values of $E_{1'2'}$ is suitable. However, the final necessary condition is $v_2' > v_1'$; which requires the first square root in eq. (2.39) to be larger than the second. Therefore, the necessary and sufficient condition in the N.R. limit for 1'2' rescattering is

$$\frac{2 \, m_3 \, Q_{R\to23}}{m_2 \, m_{23}} \geq \frac{2 \, m_{123} \, (Q - Q_{R\to13})}{m_1 \, m_{23}} \qquad [2.40]$$

in which case

$$E_{1'2'} = \frac{1}{2} \mu_{12} \left[(\frac{2m_3 \, Q_{R\to23}}{m_2 \, m_{23}})^{\frac{1}{2}} - (\frac{2m_{123} \, (Q - Q_{R\to23})}{m_1 \, m_{23}})^{\frac{1}{2}} \right]^2 \qquad [2.41]$$

The above are the necessary and sufficient conditions of the intermediate state 1'2'3 so that 1' and 2' will rescatter. For a given 23 resonance mass m_R, there is a unique value of $E_{1'2'}$ before rescattering and particle 3 has a unique speed in the overall c.m. system, but in an arbitrary direction. In the rescattering, energy and momentum are conserved, i.e.

$$E_1 + E_2 = E_{1'} + E_{2'} \quad , \quad \vec{p}_1 + \vec{p}_2 = \vec{p}_{1'} + \vec{p}_{2'}$$

Hence s is unchanged in the rescattering and therefore $E_{12} = E_{1'2'}$; i.e. the energy of relative motion of 1 and 2 -- the excitation energy of the (12) system -- is unchanged in the final rescattering and is given by eq. (2.41). However, in the rescattering, the ultimately observed particles 1 and 2 can travel in arbitrary directions compatible with energy and momentum conservation.

From eq. (2.41), one can find the interval of bombarding energies E_b where rescattering of particles 1 and 2 is possible for the given masses and an excitation energy E_{23} in the (23) system. The lower limit for E_b (EBLL) is given by

$$Q - Q_{R \to 23} = 0 \qquad\qquad [2.42]$$

where $\qquad Q = Q_1 + E_b^{Lab} \dfrac{m_t}{m_b + m_t} \qquad\qquad [2.35a]$

Q_1 is the Q-value for the reaction $b + t \rightarrow 1 + R$ and $Q_{R \rightarrow 23} \equiv$

E_{23}. The upper limit on E_b (EBUL) is given by

$$E_{12} = 0 \qquad\qquad [2.43]$$

b) Non-relativistic matrix elements

It is convenient to carry out the calculations in a

system where $\hbar = c = 1$ and to use the energy momentum four-

vector convention $P = (\vec{p}, p_{(4)})$ with $p_{(4)} = i E = i (p^2 + m^2)^{\frac{1}{2}}$.

The three body cross-section[9]) can be written as

$$d\sigma = \frac{|M|^2}{(2\pi)^4} \frac{p_{(4)b}}{p_b} \delta^4 (P_1 + P_2 + P_3 - P_b - P_t)$$

$$\frac{d^3 p_1}{(2\pi)^3} \frac{d^3 p_2}{(2\pi)^3} \frac{d^3 p_3}{(2\pi)^3} \qquad\qquad [2.44]$$

in which the normalization of Veltman[25]) has been used. The

matrix element M is composed of two parts

$$M = M_R + M_\Delta$$

where M_R represents the matrix element for the sequential decay

shown in fig. 1c, and M_Δ, that for the proximity scattering shown

in fig. 1e. The cross section of interest for comparison with

experimental data is, however, $\frac{d\sigma}{d\Omega_1 \, d\Omega_2 \, dE_2}$ which can be derived

by integrating eq. (2.44) over all unobserved quantities in the

N.R. approximation:

$$\frac{d\sigma}{d\Omega_1 \, d\Omega_2 \, dE_2} = \frac{|M|^2}{(2\pi)^{13}} \frac{m_b}{P_b} \frac{m_1 m_2 m_3 \, p_1^3 \, p_2}{m_3 \, p_1^2 - m_1(\vec{p}_1 \cdot \vec{p}_3)} \qquad [2.45]$$

Considering only s-waves in each of the vertices A, B and C, (neglecting any momentum dependence) g_A and g_B can be taken as coupling constants for vertices A and B, respectively. M_R can be written as

$$M_R = \frac{i(2\pi)^4 \, g_B \, g_A}{(2E_b 2E_t 2E_1 2E_2 2E_3)^{\frac{1}{2}}} \frac{1}{P_R^2 - m_R^2} \qquad [2.46]$$

where R is a virtual state with a finite lifetime and therefore, m_R is complex, i.e.

$$m_R = m_r - \frac{i}{2}\Gamma = m_r - \frac{i}{2\tau} \qquad [2.47]$$

in which m_r is the real mass of R, Γ is the full width at half maxima of the decaying state of the intermediate nucleus and τ, its average lifetime.

M_R contributes a resonance-like structure corresponding to a Breit-Wigner distribution.

$$P_R^2 = (E_2 + E_3)^2 - (\vec{p}_2 + \vec{p}_3)^2$$

$$= m_2^2 + m_3^2 + 2E_2 E_3 - 2\vec{p}_2 \cdot \vec{p}_3$$

$$m_R^2 = m_r^2 - \frac{1}{4}\Gamma^2 - i \, m_r \, \Gamma$$

Furthermore, from the requirement that R decays within the time interval $\bar{\tau} = \frac{1}{\Gamma}$; g_B can be written as

$$g_B = (32\pi^2 \ (m_2 + m_3)^5 \ \Gamma^2 / Q_{R \to 2\,3})^{\frac{1}{4}} \qquad [2.48]$$

The matrix element for rescattering vertex C can be written as

$$M_\Delta = \frac{g_A \ g_B \ g_C}{(2E_b 2E_t 2E_1 2E_2 2E_3)^{\frac{1}{2}}} \int \frac{d_4 \ P_R}{(P_R{}^2 - m_R{}^2)(P_1{}^2 - m_1{}^2)(P_2{}^2 - m_2{}^2)} \qquad [2.49]$$

where g_C, the coupling constant for vertex C, can be written as

$$g_C{}^{s,t} = \frac{32\pi \ \mu_{12} \ a_0{}^{s,t}}{1 + \frac{1}{2} \ r_0{}^{s,t} \ a_0{}^{s,t} \ q^2 - i \ a_0 \ q} \qquad [2.50]$$

Here, $a_0{}^{s,t}$ and $r_0{}^{s,t}$ are the scattering lengths and effective ranges for the singlet and triplet states of the deuteron, respectively. It is reasonable to assume a purely statistical distribution of the two possible spin states of the n-p system, namely a 25% admixture of the singlet state and 75% of the triplet state.

The integral in eq. (2.49) has been solved by Aitchison and Kacser[4]), in the N.R. limit, giving the following expression

$$\int = \frac{i\pi^3}{4\mu_{12}\,p} \; \ell n \left[\frac{q + \frac{pm_1}{m_{123}} + \left(\frac{2m_1 m_{23}(Q-Q_{R\to 23})}{m_{123}}\right)^{\frac{1}{2}}}{q - \frac{pm_1}{m_{123}} + \left(\frac{2m_1 m_{23}}{m_{123}}(Q-Q_{R\to 23})\right)^{\frac{1}{2}}} \right] \qquad [2.51]$$

The singularities of M_Δ arise where either the numerator or the denominator of the argument of the logarithm vanishes.

Eq. (2.51) has also been rewritten in the following two equivalent forms:

$$\int = \frac{i\pi^3}{4\mu_{12}\,p} \; \ell n \left[\frac{(q - q_N) + (m_1/m_{123})(p - p_N)}{(q - q_S) - (m_1/m_{123})(p - p_S)} \right] \qquad [2.51a]$$

and

$$\int = \frac{i\pi^3}{4\mu_{12}\,p} \; \ell n \left[\frac{q + \frac{m_1}{m_{123}}\,p - q_S + \frac{m_1}{m_{123}}\,p_S}{q - \frac{m_1}{m_{123}}\,p - q_S + \frac{m_1}{m_{123}}\,p_S} \right] \qquad [2.51b]$$

The meaning of the terms q_S, q_N, p_S and p_N will be discussed in the following section.

Substituting M_R and M_Δ in eq. (2.45), one can obtain the desired cross section in the following form:

$$\frac{d\sigma}{d\Omega_1\, d\Omega_2\, dE_2} = g_A^2 \; F\,(\Gamma, \theta_1, \phi_1, \theta_2, \phi_2, E_2) \qquad [2.52]$$

where θ_1, ϕ_1, θ_2, ϕ_2 and E_2 are the usual kinematics chosen for the "complete" experiments. The magnitude of g_A determines the absolute intensity with which the sequential decay occurs via resonance R. Through comparison with experimental data, the value of g_A is chosen to reproduce the intensity in the

principal line peak correctly. If only relative cross sections are measured, the magnitude of g_A remains undetermined.

Fitting the data with theory will then give the value of Γ, the only undetermined quantity, thereby providing a method for deriving short lifetimes.

c) Discussion of Dalitz plots

Fig. 2 shows the boundary of the allowed E_{23} vs E_{12} plots; these are known as Dalitz plots. These plots are very useful in understanding the physical aspects of the process. On such a plot, the resonance (23) system will show up as a concentration of events about a vertical line centered on $E_{23} = Q_{R \to 23}$ provided the total energy is high enough for the resonance to be produced. In fig. 2(a), the incident energy is not sufficient to produce the (23) resonance, hence there is no effect at all. Fig. 2 (b) represents the case where the rescattering condition (2.40) is satisfied, the line $E_{23} = Q_{R \to 23}$ being to the right of the point b.

Of the two values of E_{12}, namely E_{12S} and E_{12N} given by the points S and N, respectively, only the one at S permits rescattering, whereas E_{12N} corresponds to the particles 1 and 2 being anti-parallel to each other.

q_S, q_N, p_S and p_N are, then, given by the values of q and p corresponding to the points S and N respectively. M_Δ in eq. (2.51a) becomes infinite, logarithmically, for $q = q_S$, since $p = p_S$ when $q = q_S$. Therefore, if the total energy and

a

E_{12}

d

c

a

b

$E_{23} = Q_{R \to 23}$

E_{23}

$\to \Gamma \leftarrow$

E_{12}

E_N

d

N

b

c

a

S

E_S

b

$E_{23} = Q_{R \to 23}$

E_{23}

E_{12}

d

c

a

b

$E_{23} = Q_{R \to 23}$

E_{23}

c

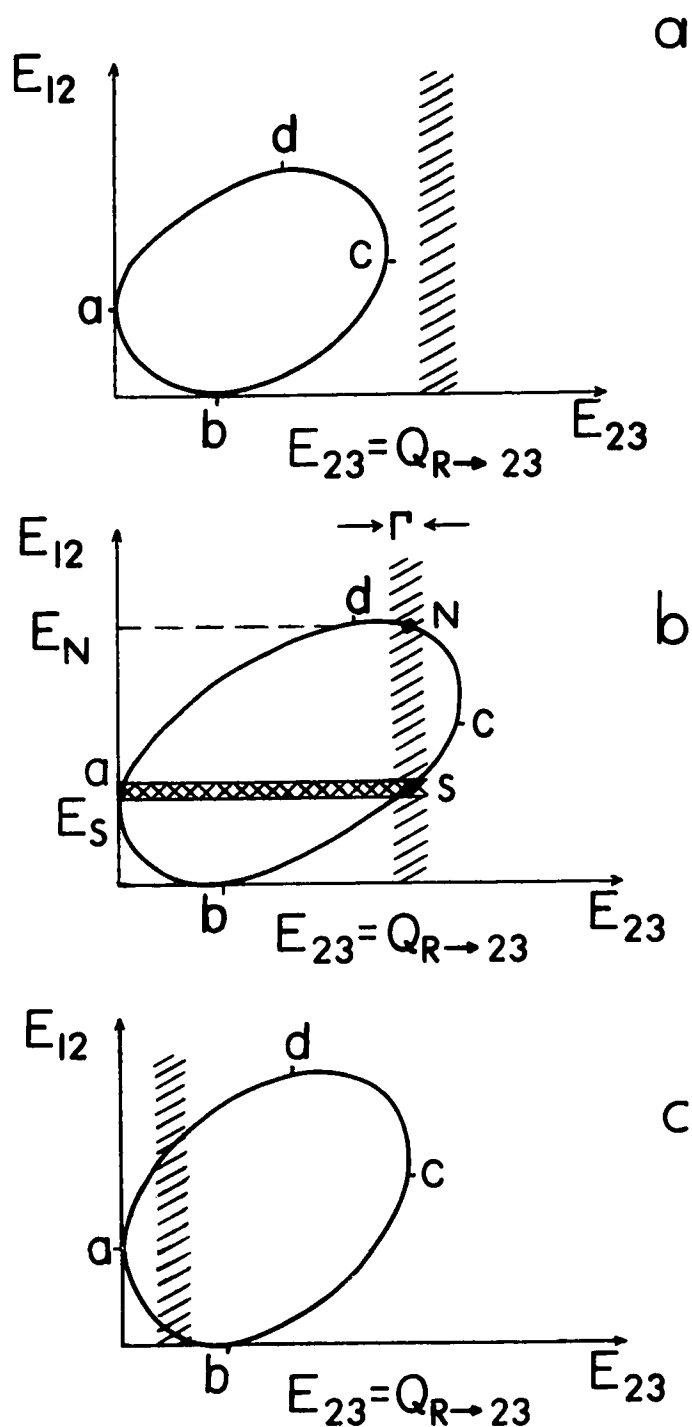Figure 2   Dalitz plots showing the N.R. kinematic conditions for rescattering for various bombarding energies E_b. The relevant arc is bc in each case. a) E_b is below the threshold for R; b) E_b is satisfactory for real rescattering corresponding to point S, leading to the shaded band corresponding to E_S.The width of (23) resonance is indicated by Γ; c) E_b is too large.

masses of the resonance and of the particles are such that a resonance line E_{23} intersects the lower right hand arc of the Dalitz plot, then the amplitude will show a logarithmic enhancement in q near the point of intersection, due to M_Δ. Because this singularity is near the physical region, a rapid variation in the amplitude should be observable.

In fig. 2 (c) , the incident energy is too high, therefore the E_{23} line crosses the Dalitz plot on the lower left hand corner where the rescattering condition (2.40) is not satisfied, i.e. the velocity $\vec{v}_2'$ is not greater than $\vec{v}_1'$. Hence, no proximity scattering is possible in this case.

The width of the intermediate resonance, Γ, also plays an important role in this process. From fig. 2, one can see that line E_{23} has a spread corresponding to the width Γ of the resonance. If Γ is large, there will be a large uncertainty in the spread in q_S. Physically a large Γ means a short lifetime for the resonance, so it will, presumably, not move far from the production vertex before it decays (hence the name "proximity scattering"). So, by the uncertainty principle, there is a large spread of momenta associated with its decay products, and hence a large spread of possible configurations in which the rescattering is kinematically allowed. This corresponds exactly to intersecting the Dalitz plot with a "woolly" E_{23} line. If the width is small, there will essentially be only one unique configuration of particles in the final state for which the rescattering is

allowed -- and this corresponds to an intersection of the boundary by a sharp E_{23} line. Consequently the logarithmic singularity is expected to be sharply defined. On the other hand, we see from the formula for M_Δ (eqs. 2.49, 2.51a) that g_B, which has a $\Gamma^{\frac{1}{2}}$ dependence, multiplies the log function -- and this is easily understandable, because if the lifetime is very long (Γ small) the resonance will not decay at all. Thus for small Γ the probability of rescattering will also be very small.

Finally, remarks about the factors not considered in the above formalism are in order. All the time we have assumed only s-waves. Another simplification lies in the fact that the particles have been considered as spinless. For a general case of particles with spin, polarization vectors must enter, suitably coupled with momenta which give rise to both angular factors and angular momentum barrier factors. Hence g_B changes from a constant to a well defined and fairly straight forward function of three-momenta of the particles 2 and 3, and the various polarization vectors. However, these assumptions do not significantly affect our results[4]). Lastly, the effects long-range forces, such as those associated with the Coulomb interaction, have been neglected.

CHAPTER 3

EXPERIMENTAL APPARATUS AND PROCEDURES

3.1 Incident Beam

The incident deuteron beam for this study was provided by the University of Alberta 7.5 MeV CN van de Graaff Accelerator.

3.2 Scattering Chamber

A 24" diameter stainless steel scattering chamber consisting of a 1" thick base plate and a bell jar was designed and fabricated for this study. A target mount capable of holding three targets was attached to a pillar passing through a 2" diameter port at the centre of the base plate. The vertical and horizontal position of the target as well as its angle to the incident beam could be remotely controlled and read out using a digital voltmeter. A lucite flange with vacuum tight BNC-feedthrough connectors was screwed onto a 4" diameter recess in the base plate. Coaxial cables were connected through these connectors to supply the detector bias as well as for the output pulses from the solid state detectors. Such a flange was helpful in grounding the cables only in the control room where the rest of the circuitry was located, thereby reducing the high frequency noise pickup.

The beam was collected by a gold lined, brass Faraday cup, $\frac{3"}{4}$ in diameter and 6" long. This cup was screwed onto the base plate

at 0° and was electrically insulated from it. Cooling to the cup was supplied by circulating air in the copper tubing soldered to its walls. A negatively biased guard ring was provided to suppress the secondary electrons from the Faraday cup. The current integrator input was taken from a lead attached to the cup.

3.3 Detector 2π-Positioning Mechanism

Fig. 3 shows a photograph of the scattering chamber and the 2π-positioning mechanism for the solid state detectors. By means of this mechanism, a detector could be placed at any angle either in the horizontal or in the azimuthal plane with an accuracy of 0.1°.

This mechanism was supplied by Ortec and was a modification of their Model 648, especially fabricated to fit into our scattering chamber. It consisted of an aluminum ring ($\frac{1}{2}$" thick with a 20 $\frac{5}{8}$" O.D.) mounted on three pillars rigidly attached to the base plate at 45°, 107.5° and 180° respectively. The pillar at 180° had a 2" diameter hole through which the beam could pass. An inner aluminum ring was suspended by means of nylon wheels which could move in a tapered grove on the inner surface of the outer ring. The movement of this inner ring was controlled by a motor-drive and it was capable of rotating from 0° to 360° in the horizontal plane. A semicircular arc was fixed to the upper surface of the inner ring and a motor truck assembly could move along this arc by means of another motor-drive with an elevation range of 0° to 90°.

Figure 3   Photograph of experimental arrangement showing the scattering chamber, detector 2π-positioning mechanism, detectors, faraday cup and collimators, etc.
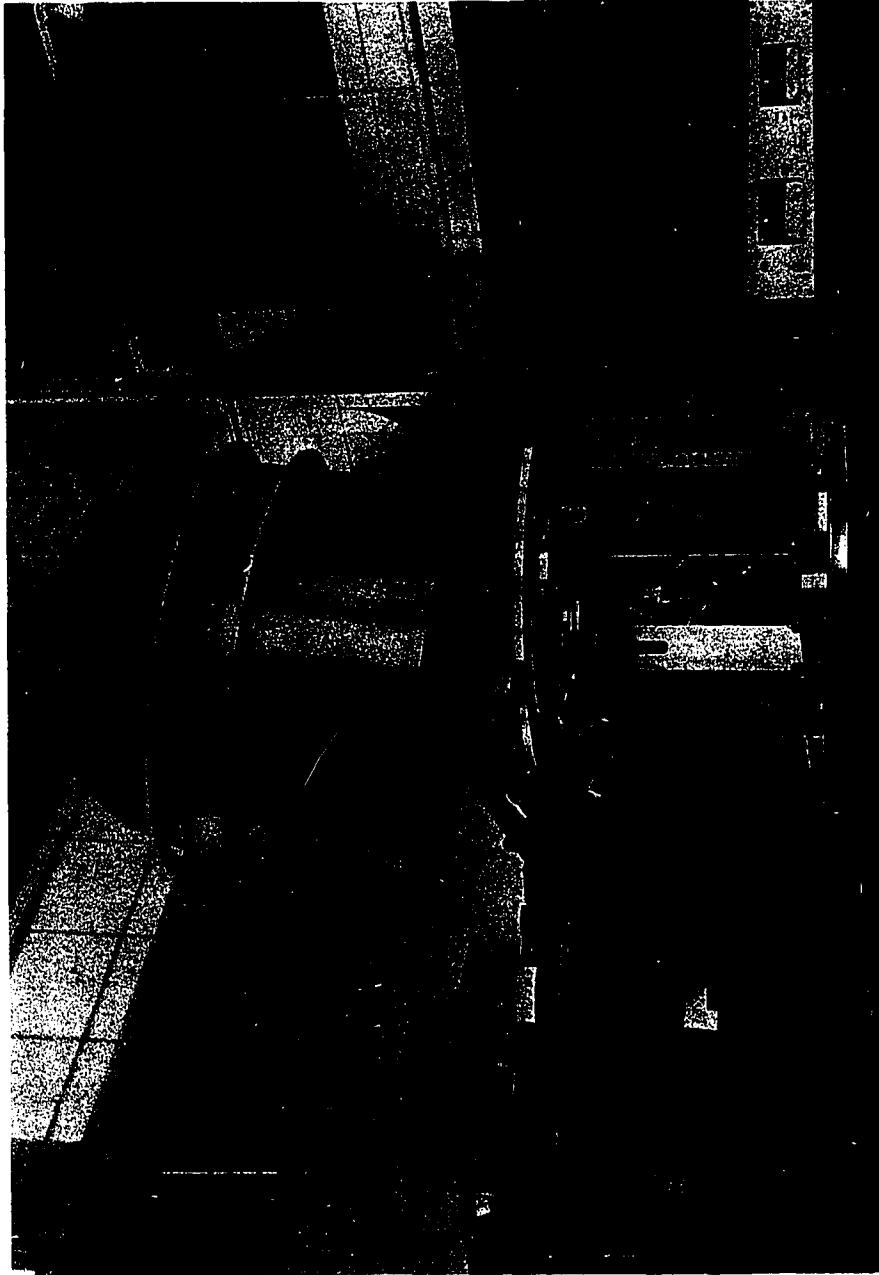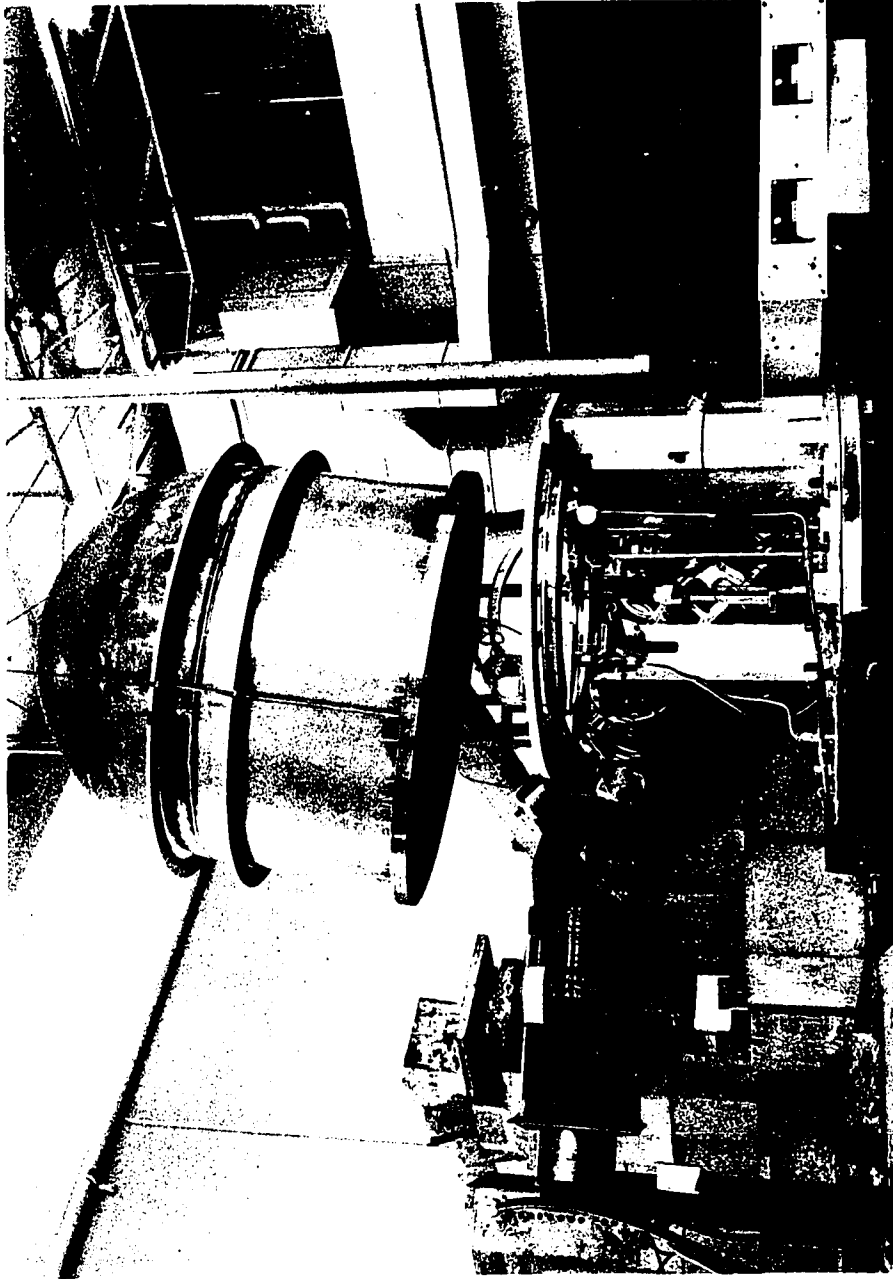
Figure 3 Photograph of experimental arrangement showing the scattering chamber, detector 2π-positioning mechanism, detectors, faraday cup and collimators, etc.

A detector holder with a set of collimators was attached to this motor truck assembly so that in any position of elevation, the detector was always pointing towards the centre of the target.

The drive motors could be operated through a remote control unit supplied with the 2π-positioning mechanism. This unit essentially consisted of two individual units in one chassis with a common pulse generator. The drive motors were driven with square wave pulses from the pulse generator. The output from the pulse generators was amplified by two identical dc amplifiers which drove the motors with 30 v pulses. The speed of the drive motor was determined by the generator frequency. The mechanical registers were advanced or retarded by pulses generated from a contact wheel located on each motor assembly.

3.4 Targets

Self supporting targets were made in the laboratory by evaporation. Silicon targets for the (d,np) reaction were fabricated by evaporating SiO_2 powder onto the glass slides on which a very thin layer of NaCl was deposited in a prior evaporation. As Silicon has a very high melting point, a rather high current ($\simeq$ 200 amperes) was applied to a Tantalum boat containing SiO_2 powder. Some Ta from the boat also evaporated, which proved rather helpful because the (d,d) elastically scattered peaks from Ta could be used for the energy calibration of the charged particles.

The same method was followed in preparing carbon targets, except that the e-gun was used to disintegrate a piece of natural carbon (abundances: 98.982% ^{12}C, 1.108% ^{13}C).

After evaporation, these targets were floated off the glass plates by slowly and carefully immersing them into a tub of water in an inclined position; subsequently they were picked up on a metal frame. The thickness of these targets was estimated to be approximately 100 μgm/cm^2.

For the ^{7}Li(d,α)αn experiment, two kinds of targets were made. The first kind were obtained by evaporating a thin layer of Li F onto an aluminum foil approximately 170 μgm/cm^2 thick, while the second type were made by the in situ evaporation of ^{7}Li metal on a carbon backing.

The ^{13}C targets with 95.7% isotopic enrichment were supplied by Penn Spectra-Tech, Inc. of Wallingford, Pa., U.S.A. Thickness of these targets were 75 and 150 μgm/cm^2.

Thin deuterated polyethelene foils were supplied by Micro Matter Co. of Seattle, Washington, U.S.A. This foil was bombarded by 4 MeV deuterons to provide n-^{3}He coincident pairs used to set up the electronics for coincidences between neutrons and charged particles.

3.5 Detectors

a) The charged particle detector used for most of the runs for the ^{12}C(d,np)^{12}C reaction was an Ortec - 130 surface barrier

detector-preamplifier timing system which is optimized for both energy and time resolution. Two distinctly different outputs -- the timing and energy signals -- are provided on separate output connectors for independent processing. Alpha resolution of this detector was < 20 keV FWHM, whereas the timing resolution was < 250 p s ec FWHM for a fast light-pulse generator calibrated to an energy of 5.47 MeV.

The detector was attached to a detector holder assembly and was placed at a distance of 5" from the target. A set of two circular Ta collimators (front: $\frac{1}{2}$" in diameter, back: $\frac{3}{10}$" in diameter) separated from each other by 2" was placed in front of the detector and served as a telescope to eliminate detection of particles scattered from points other than the beam spot. The back collimator defined the solid angle subtended at the centre of the target.

To study the $Li + d \rightarrow n + \alpha + \alpha$ reaction, two thin solid state surface barrier detectors were used. One of the detectors was attached to the positioning mechanism while the other was mounted on the top of a pillar attached to the base plate. The experimental set up for this experiment is shown in fig. 4.

b) During some of the initial runs on the $^{12}C(d,np)^{12}C$ reaction as well as while studying the $^{28}Si(d,np)^{28}Si$ reaction a 1,000 μ thick totally depleted surface barrier detector was used. An Ortec - 113A preamplifier was used for the energy pulses whereas
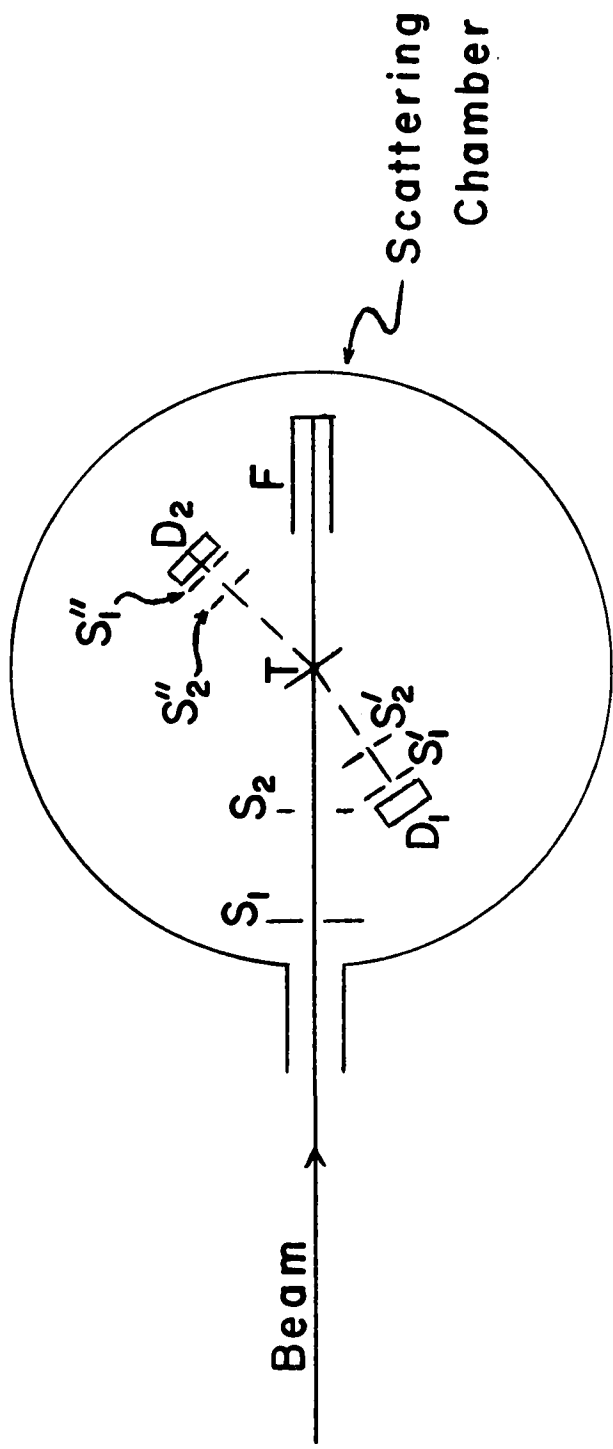
Figure 4   Experimental arrangement for the $^7Li(d,n\alpha)\alpha$ reaction. Slit S_1 defines the beam, S_1' and S_1'' define the solid angle and S_2, S_2' and S_2'' are anti-scattering slits. F is the faraday cup, D_1 and D_2 are solid state detectors and T is the target.

a fast low noise preamplifier[39]) was used to derive the timing signal.

c) The neutrons were detected by a Ne 213 liquid scintillator, $3\frac{1}{2}"$ in diameter and 2" in depth, mounted onto an RCA 8854 photo-multiplier tube assembly. A 2" thick lead shielding was placed inside the scattering chamber in such a manner that it minimized the detection of neutrons and gamma rays incident on the detector from directions other than directly from the target. The typical distance of the neutron detector was 45 cm from the centre of the target. The detector was mounted on a remotely controlled trolly and its distance as well as angle could be varied and accurately determined by means of a digital voltmeter located in the control room. Experimental set up for the (d,np) experiments is shown in fig. 5.

3.6 Detector Efficiencies

The detection efficiency of the charged particle detectors and their associated circuitry was taken as 100%.

The neutron detectors not only have low efficiency, but also their efficiency varies drastically at neutron energies below 1 MeV. Since the shape of the detection efficiency versus neutron energy curve is particularly sensitive to the detector bias setting at neutron energies close to the counter threshold, an accurate measurement of the threshold setting is of great importance.
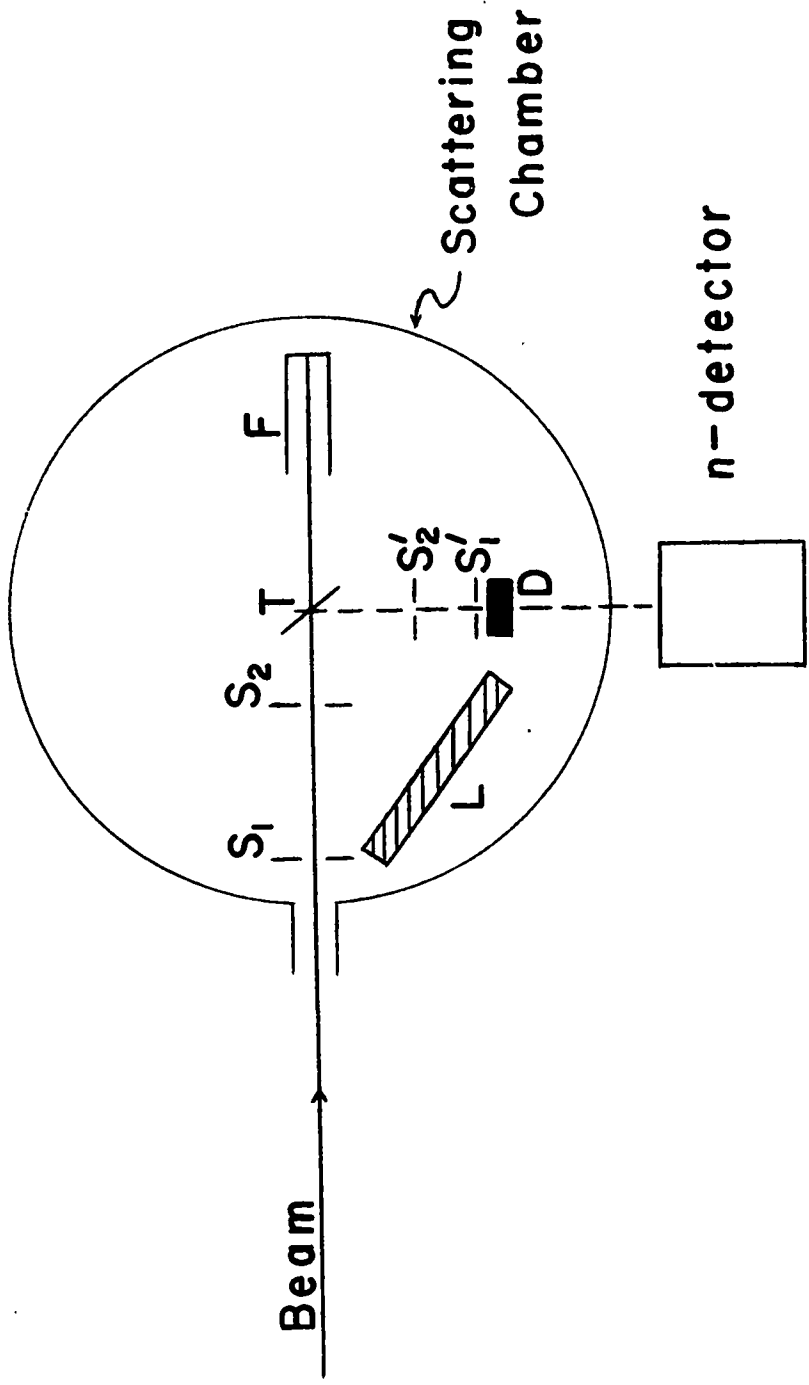
Figure 5   Experimental arrangement for the $^{12}C(d,np)^{12}C$ reaction. L is lead shielding. Other details are the same as for fig. 4.

The lower threshold of the neutron detector was carefully measured, and checked before and after the runs, using the standard electronics configuration. The technique is discussed in detail, elsewhere[40]). The typical value of the threshold corresponded to $\sim$ 250 keV proton energy.

The efficiency versus neutron energy curve for a Ne 213 scintillator given by Lindstrom et al.[41]) very closely matched our experimental conditions. This curve was then used to correct our data for the neutron detector efficiency.

3.7 Pulse Shape Discrimination (PSD)

Neutrons and gamma rays produce light scintillation in organic scintillators with significantly different decay characteristics[42]). This difference in pulse shape is utilized to distinguish between gammas and neutrons, thereby reducing the background due to gamma rays in the detector without substantially lowering the neutron detector efficiency.

Pulse shape discrimination was done by comparing the time difference between fast leading edge trigger and cross over time of the pulse obtained from a double delay line shaping amplifier (see fig. 6).

3.8 Circuitry

A typical block diagram of the circuitry used to study the (d,np) reaction is shown in fig. 6. The deuteron beam was incident
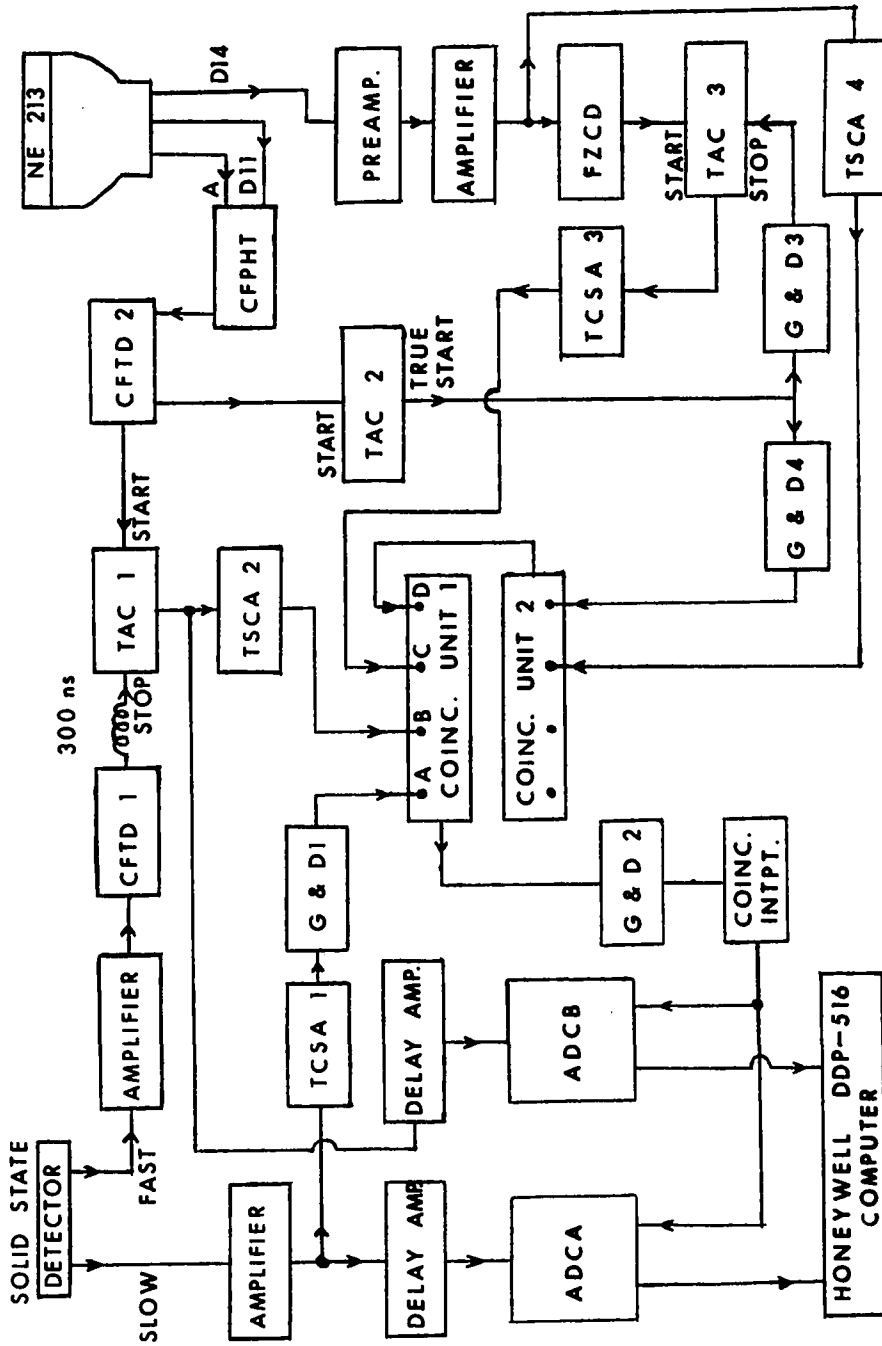
Figure 6   Block diagram of electronics.

on the ^{12}C target and the neutrons and protons were detected by a Ne 213 scintillator and a solid state detector, respectively.

Slow pulses from the Ortec - 130 surface barrier detector and preamplifier assembly were fed into a Canberra 1411 double delay line clipped amplifier. The bipolar output of this amplifier was divided into two parts. Part one: after being suitably delayed in an Ortec 427 delay amplifier, was sent to analog-to-digital converter A (ADCA); part two: was fed into a timing single channel analyzer (TSCA, Ortec - 420), where the appropriate energy interval of protons was selected. The output of this TSCA, after passing through a gate and delay generator (G & D, Ortec - 416), was sent to terminal A of the universal coincidence unit (Ortec - 418).

Fast pulses from the Ortec - 130 were used as the input to an Ortec - 454 timing filter amplifier, the output of which was fed to an Ortec - 453 constant fraction timing discriminator (CFTD). The lower threshold was set in the 453 to eliminate noise and the walk was properly adjusted. The output of this CFTD was delayed by 300 ns and then used as the stop pulse for a time-to-amplitude converter (TAC 1, Ortec 437A).

The anode and eleventh dynode outputs from the photomultiplier tube coupled to the neutron detector were fed into a constant fraction pulse height trigger[43]) (CFPHT) which provides the optimum time resolution with a scintillator photomultiplier system over a 100:1 dynamic range. The residual walk over the

same pulse height range is within ± 120 psec, whereas the lower threshold is variable from 0.8 mA to 10 mA on the anode pulse height. The input to CFTD #2 was taken from CFPHT, and its output was used to start the TAC #1, the output of which (the time spectrum pulse) after going through a delay amplifier (Ortec - 427) went to another analog-to-digital converter (ADCB). The window on the time spectrum was suitably selected by a TSCA (Ortec - 455), the output of which was fed to terminal B of the universal coincident unit (Ortec - 418).

The neutron energy pulse was taken from dynode 14 of the photomultiplier tube and after passing through a preamplifier (Ortec 113) went to a delay line amplifier (Ortec 460). After proper shaping and amplification, the bipolar output of this amplifier was divided into two parts; one part was used for PSD whereas the other part was used for energy selection by means of a TSCA (Ortec - 455). The output of this single channel analyser went to another universal coincident unit (#2) which was used for slow-fast coincidences. The fast pulse came from CFTD #2. The output of universal coincidence unit #2 was fed to the terminal D of the coincidence unit #1, and terminal C was connected to the output from the PSD circuit.

The four way coincidence output of unit #1 was then fed into the gate and delay generator #2 (Ortec - 416), and its output was used as a gating pulse for ADCA and ADCB. Finally, the signals from ADCA and ADCB were read into a Honeywell DDP-516 computer

where they were stored in a two-dimensional array of 128 x 128 channels.

To study the ^{7}Li(d,α)αn reaction, two solid state detectors were used to detect the alpha particles and the circuitry was modified accordingly. Coincident events were determined using fast signals from the detectors to start and stop a TAC. The TSCA was set around the time region of interest and the output from this was used to open gates through which the energy signals from the detectors were routed. The events were stored in the computer in a two-dimensional array of 128 x 192 channels.

3.9 Computers

A Honeywell DDP-516 computer was used for on-line data acquisition. The data were processed using the IBM 360/67, SDS-920 and Digital - PDP8/e computers.

CHAPTER 4

INVESTIGATION OF PROXIMITY SCATTERING

4.1 The $^7Li(d,n)^8Be^*_{16.63}(\alpha)$ α Reaction

a) Introduction

The first study of the reaction $^7Li(d,n\alpha)\alpha$ was reported by Valkovic et al.[12]). They performed the measurements, at deuteron bombarding energies E_d = 3.0, 3.2 and 3.6 MeV, in an effort to look for proximity scattering between the neutron and an alpha particle being emitted by the resonant ^8Be system. The alpha particles were detected in coincidence at the laboratory angle settings of θ_1 = 30° and θ_2 = 140° with respect to the beam direction.

There is also a possibility of neutron-alpha particle rescattering in the $^7Li + d \rightarrow \alpha + \alpha + n$ reaction. In this case the reaction will proceed as $^7Li + d \rightarrow \alpha + {}^5He^*_{16.7} \rightarrow \alpha + n + \alpha$. Fig. 7 shows the energy level diagrams for ^8Be and ^5He systems. Valkovic et al. looked for rescattering between the first emitted alpha particle and the neutron emitted from the decay of 16.7 MeV state in ^5He. The experiment was performed at an incident deuteron energy E_d = 5.9 MeV and angle settings θ_{α_1} = 40°, θ_{α_2} = 110°. From the measured α-α coincidence spectra they concluded, in both of the above cases, that the contribution due to rescattering effect was insignificant.

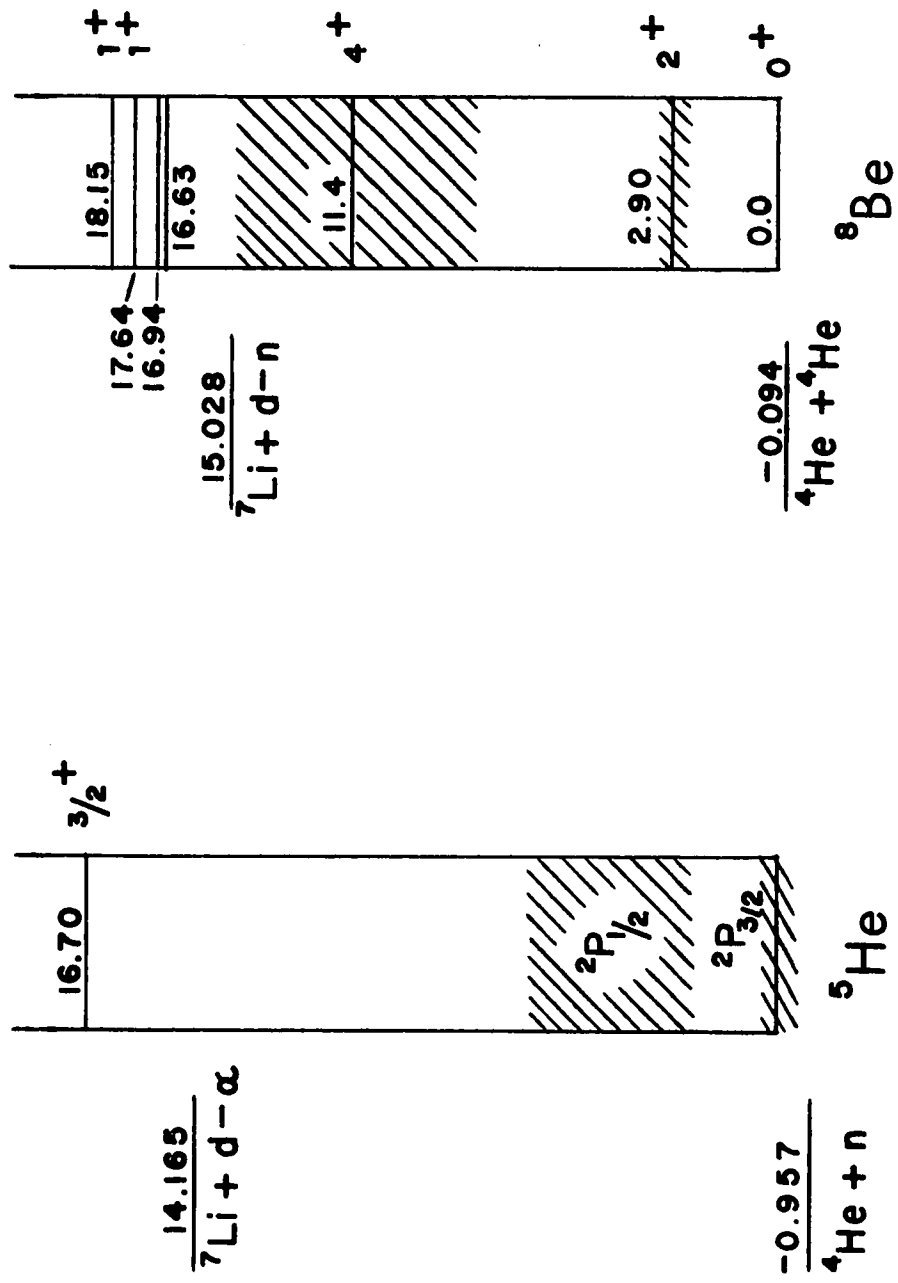Figure 7   Level diagram for ^{8}Be and ^{5}He.

However, in a subsequent study of the reaction by Thiévent et al.[13]) at incident energies between 2.07 and 2.25 MeV, the results showed a clear dependence of the proximity scattering on the incident deuteron energy. The data reported by these authors at 2.07 and 2.09 MeV deuteron energies are shown in fig. 8, and contain a rather large enhancement from the proximity scattering which is very different from that seen in n-prescattering results. In the latter, the rescattering runs over a wide range of $p-^{12}C$ relative energies $(E_{p^{12}C})$; this spread is related to the widths of the resonant states in the $p + ^{12}C$ system. In view of the implications which "strong" rescattering effects attributed to proximity scattering in the $^7Li + d$ reaction may have on the analysis of the data in the $^{12}C + d$ and $^{40}Ca + d$ reactions, further verification of n-α rescattering was undertaken as a part of the present study.

b) Experiment

The experimental set up has been described in Chapter 3 and is shown in fig. 4. Because of the large variation, due to angle and energy dependence, of the position on the kinematic locus where one would expect to see rescattering events, it was necessary to take a number of precautions. To ensure that spreading due to finite angle acceptance would not disperse rescattering events appreciably, the angular acceptance of both detectors was restricted to ± 0.5° in the rescattering plane, and ± 1.5° in the azimuthal direction. The beam energy calibration was checked by a measurement
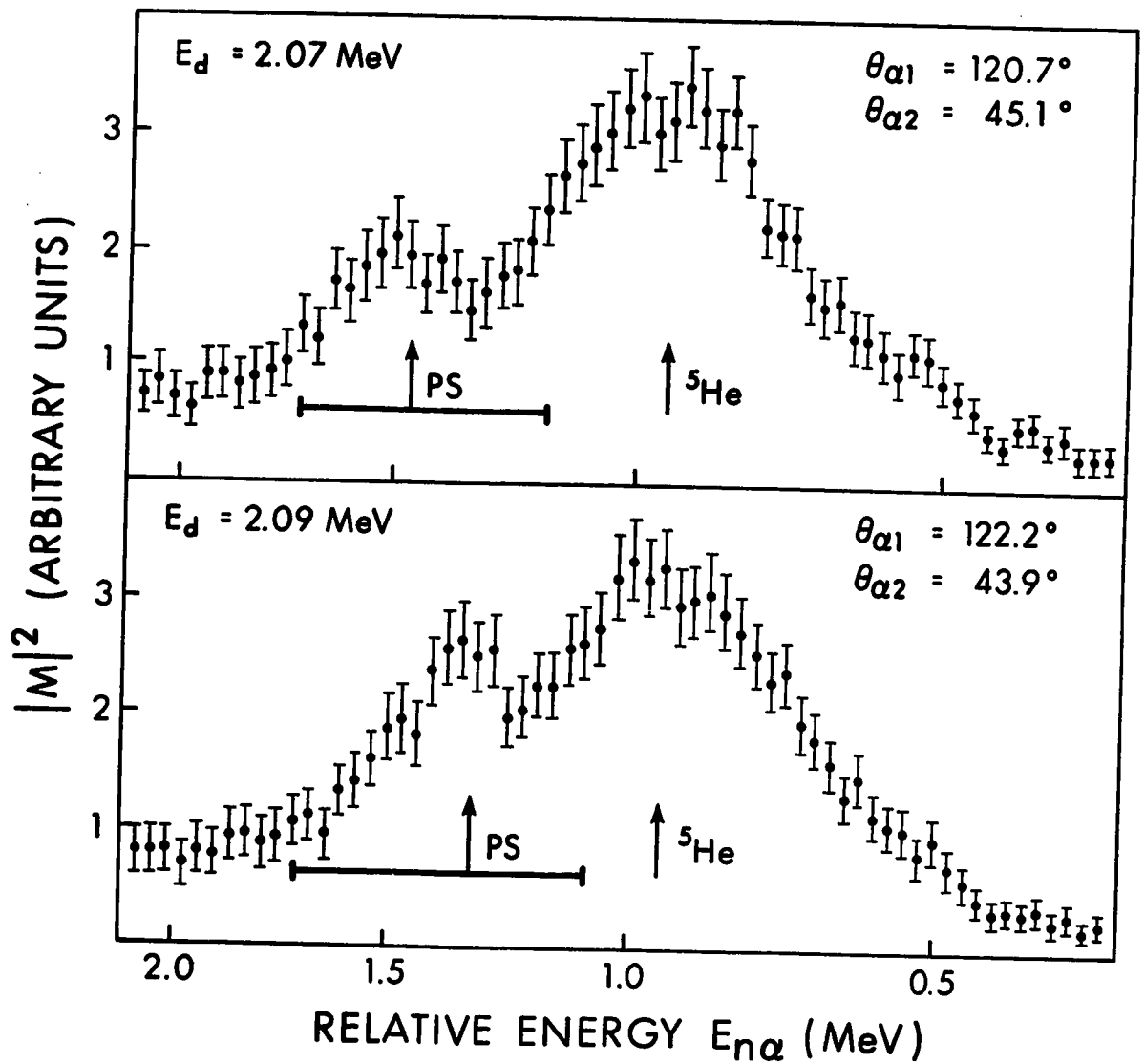
Figure 8   The 2.07 and 2.09 MeV data of Thiévent et al.[13] for the $^7Li(d,n\alpha)\alpha$ reaction. The arrows indicate the expected positions of the peaks corresponding to the decay of the g.s. of ^5He and to the 'centre' of the proximity scattering (P.S.) enhancement. The horizontal lines have been added to suggest the extent of the expected enhancement due to the width of the ^9Be (16.63) state.

of the 1.8806 MeV threshold of the $^7Li(p,n)^7Be$ reaction which is very close to the energies used in this experiment. This resulted in a determination of the absolute beam energy to an accuracy of 2 keV. Close to the threshold for rescattering, the relative energy $E_{n\alpha}$ varies very rapidly as a function of the incident beam energy as shown in fig. 9. It was thus necessary to know very accurately the incident deuteron energy spread due to finite target thickness. This was determined for the LiF target by measurement of the resonance at E_p = 1348 keV in the reaction $^{19}F(p,\alpha\gamma)^{16}O$, which is known to have a width Γ < 6 keV. These measurements were made using a technique described elsewhere[44]). The resultant yield curve showed that the energy loss for 1.3 MeV protons in the LiF target was about 6 keV, which corresponds to about 7 keV for the 1.9 - 2.1 MeV deuterons used in the rescattering measurements. Target thickness of the second target (^7Li target) used was continuously monitored while the in situ evaporation took place during incident beam bombardment of the carbon foil. In terms of the total deuteron energy loss, the final ^7Li thickness was of the same order as that of the LiF target. Both targets gave the same results for the $^7Li(d,n\alpha)\alpha$ reaction. In addition, they both contained ^{16}O as an impurity. The significance of ^{16}O contamination will be discussed in section 4.1 (d).

The width of the time region in which real events occurred was about 20 nsec. This was due mainly to the difference in flight times of the alpha particles. This fundamental limitation on the deter-
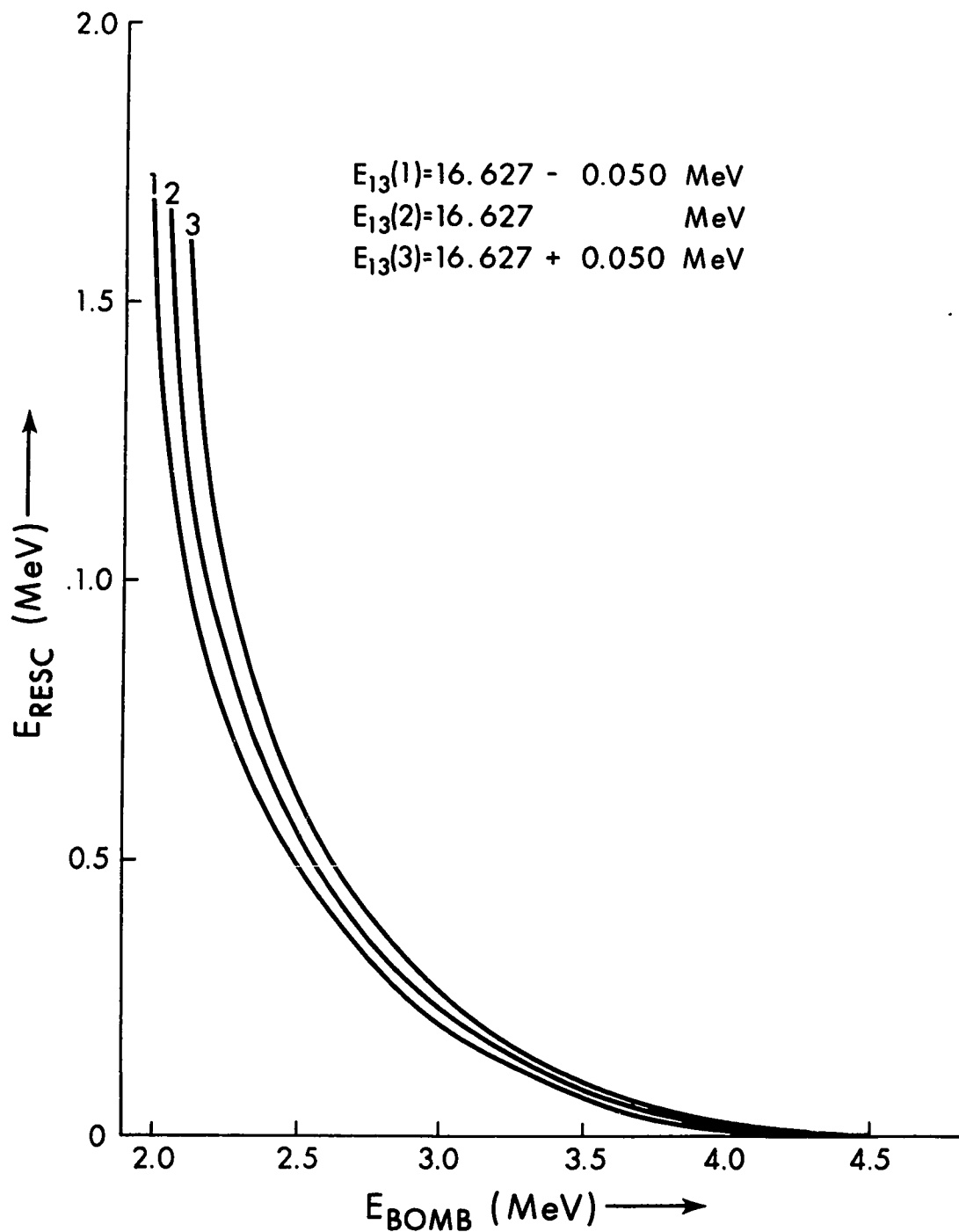
Figure 9   The variation of the rescattering energy, E_{resc}, with incident particle bombarding energy, E_{Bomb}, for the $^7Li(d,n\alpha)\alpha$ reaction. Curves 2, 1 and 3 correspond to the ^8Be (E_R = 16.63) state, $E_R - \Gamma/2$, and $E_R + \Gamma/2$ resonance energies respectively.

mination of the simultaneity of events resulted in a small but important contribution due to accidental events. Separate runs were taken with a time window placed around a region away from the real time peak and the contributions due to accidentals determined. The importance of the results obtained is also described in section 4.1 (d).

Calibration of both energy axes was performed by recording singles energy spectra for the $^7Li(d,\alpha)^5He$ and the $^{19}F(d,\alpha)^{17}O$ reactions at a number of angles and from the $^7Li(d,n\alpha)\alpha$ kinematic locus itself.

c) Results

The kinematic locus for the reaction $d + ^7Li \to \alpha + \alpha + n$ for a deuteron bombarding energy of 2.07 MeV and detector angle settings $\theta_{\alpha_1} = 120°$, $\theta_{\alpha_2} = 45°$ is shown in fig. 10. The positions where enhancement, due to relevant states in the mass 5 (^5He) and mass 8 (^8Be) systems, would be expected, are also indicated on this figure. The large decay widths of these states result in a spreading of the enhancement along the kinematic locus; each area shown encloses the section of the locus where the relative energy of the particular resonant particle is within the range $E_R \pm \Gamma/2$, E_R being the energy of the resonance and Γ the particle decay width. The positions at which proximity scattering would occur in the "classical" approach for an intermediate state of 16.63 MeV in the ^8Be system are also indicated.
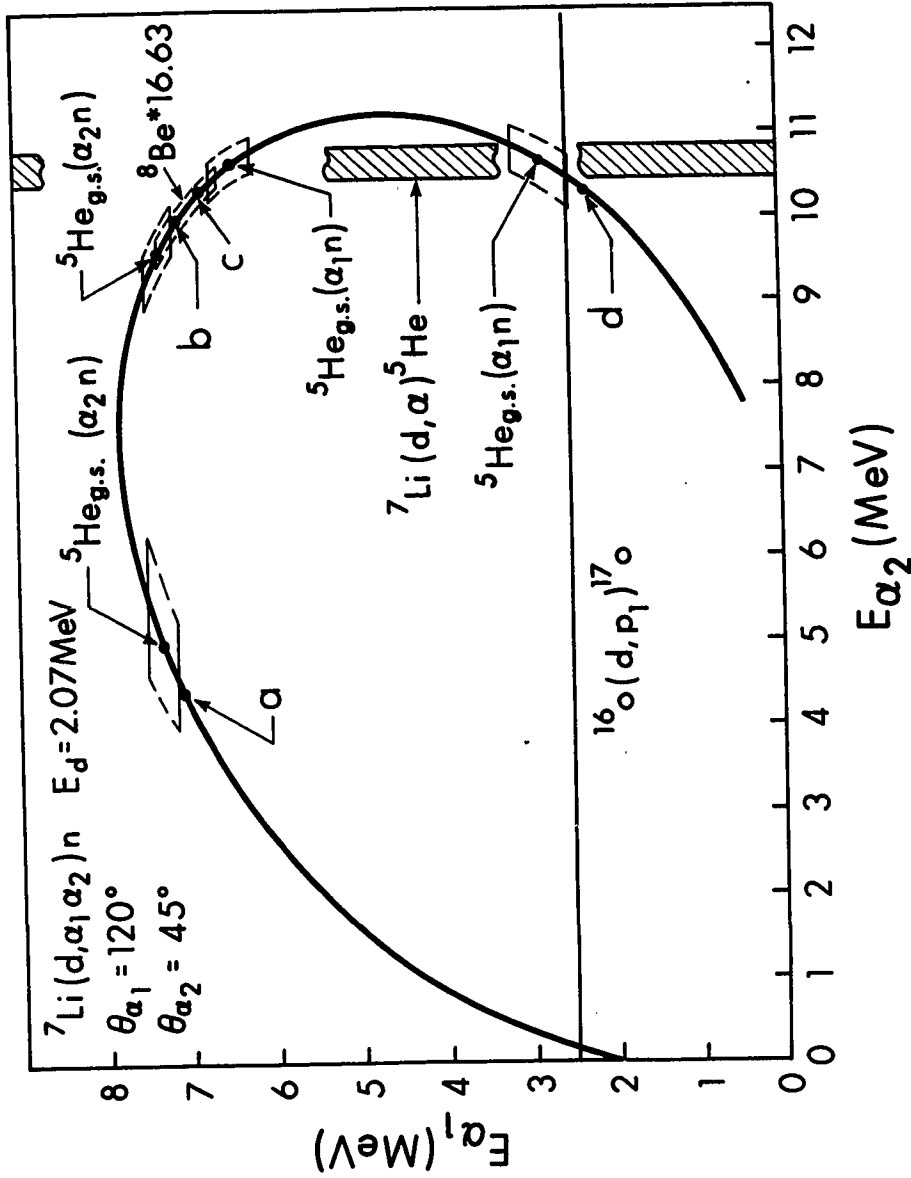
Because rescattering can occur between either of the alpha

Figure 10 The kinematic locus for the reaction $^7Li(d,n\alpha)\alpha$ at $E_d = 2.07$ MeV. The locations of expected enhancements due to n-α rescattering via the 16.63 MeV state of ^{8}Be are marked a, b, c, d. Also shown are the location and approximate extent of the ^{5}He (g.s.) and ^{8}Be (16.63 MeV state) enhancements attributed to sequential decay processes. The horizontal line labelled $^{16}O(d,p_1)^{17}O$ and the vertical shaded region labelled $^7Li(d,\alpha)^5$He represent expected "accidental" coincidence events due to the "singles" rates in the two detectors.

particles and the neutron, there are four points on the kinematic
locus at which the relative energy in the neutron-alpha system,
$E_{n\alpha}$, is equal to E_{resc}. Each of these points, labelled a to d
in fig. 10, may be characterized by (i) the C.M. angle of the
neutron emitted in the $^7Li(d,n)^8Be^*$ reaction before the rescatter-
ing and (ii) the "effective C.M." scattering angle of the rescat-
tered α-particle with respect to the $n(\alpha,\alpha)n$ proximity scattering
process. Locations a and b correspond to the same value of the
former angle (in this case approximately 50°), but different
values of the latter (in this case almost 180° for a and 0° for
b). Similarly, locations c and d correspond respectively to
the approximate angles (130°, 0°) and (130°, 180°).

The data for E_d = 2.07 MeV are shown in fig. 11 as projections
onto the E_{α_1} and E_{α_2} axes. The spectra are seen to be dominated by
the sequential decays through the ^5He ground state and the 16.63
MeV state in ^8Be.

The region where one may expect proximity scattering is
reproduced, for the 2.07 MeV data and for measurements made at
incident deuteron energies of 2.08 and 2.09 MeV, on an enlarged
scale in fig. 12. Only the two regions where proximity scattering
occurs well removed from the ^8Be resonance (positions a and d of
fig. 10) are shown in this figure. Data are plotted as a function
of $E_{n\alpha}$ and have been projected perpendicularly to the kinematic
locus. The expected positions for rescattering from the centroid
of the 16.63 MeV level are marked by arrows. The horizontal lines

have been drawn to suggest the range of values of E_{resc} ($\equiv E_{n\alpha}$) over which the proximity scattering may be expected when the finite width of the ^{8}Be (16.63) state is taken into account (see fig. 9).

The lower limit on the incident deuteron energy for which proximity scattering is possible in the ^{7}Li + d reaction is 2.061 MeV if one takes E_{23} to be the centroid of the 16.63 MeV level (see eq. 2.42). The lower limit is however decreased when one considers the width of the ^{8}Be resonance, as can be seen from fig. 8. Measurements have been made at incident energies of 2.05 and 1.90 MeV to obtain a line shape for the ^{5}He resonance which could not be affected by rescattering. (Actually, at 2.05 MeV some proximity scattering via the "low energy end" of the 16.63 MeV state is possible, but one would expect a greatly reduced effect. At 1.90 MeV the rescattering would be negligible.) The results of these measurements for θ_{α_1} = 120° and θ_{α_2} = 45° are shown in fig. 13. To allow comparisons to be made between line shapes for the peak at 1.90 MeV and at high energies, a Monte Carlo simulation was used to fit a Breit-Wigner resonance shape plus linear background to the 1.90 MeV data. The same resonance parameters were then used to predict the shapes to be expected at the higher energies. The resultant shapes for 1.90, 2.05, 2.07, 2.08 and 2.09 MeV are shown, together with the measured spectra, in fig. 14. It is evident that all the spectra are well reproduced in this manner.
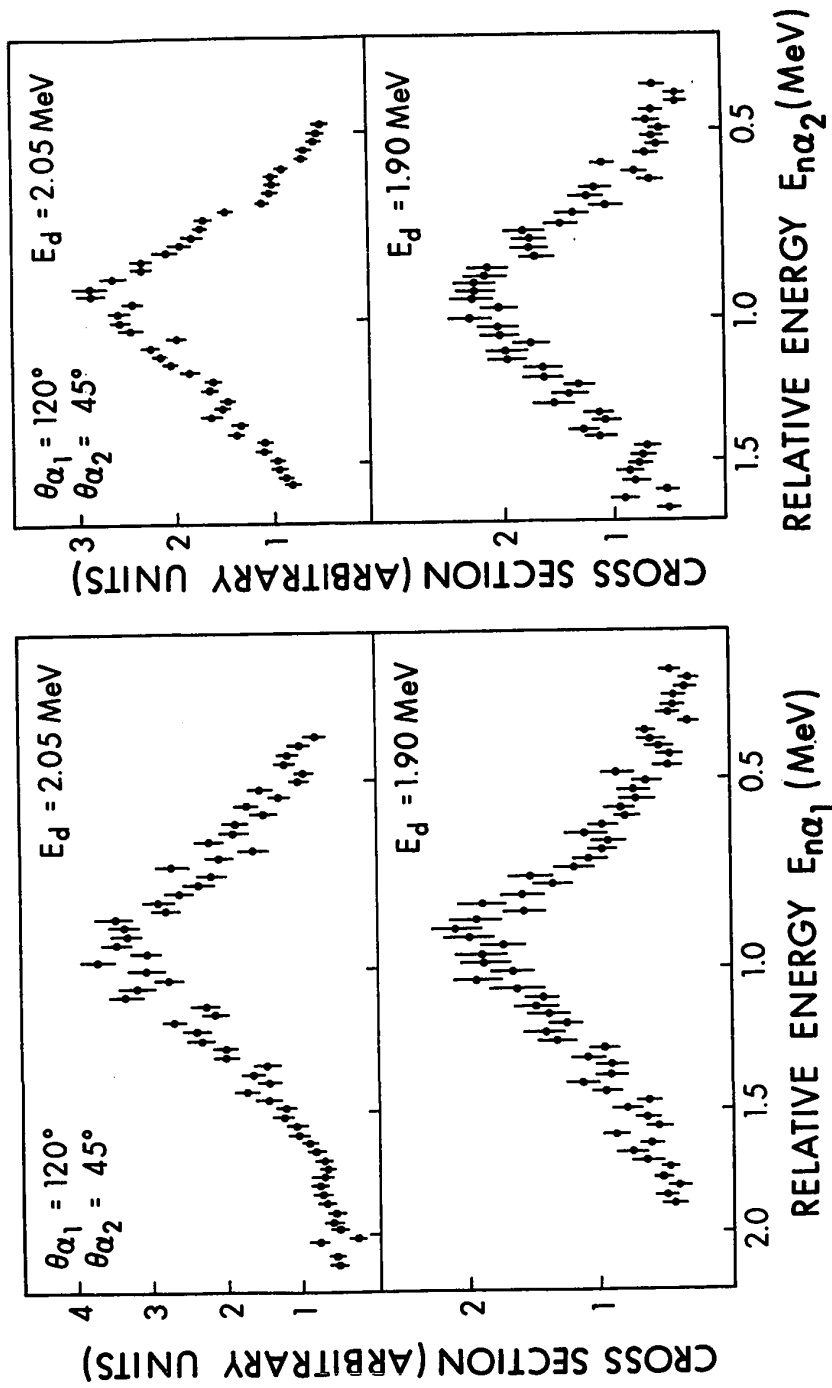
Figure 13   As for fig. 12, except that E_d = 1.90 and 2.05 MeV.
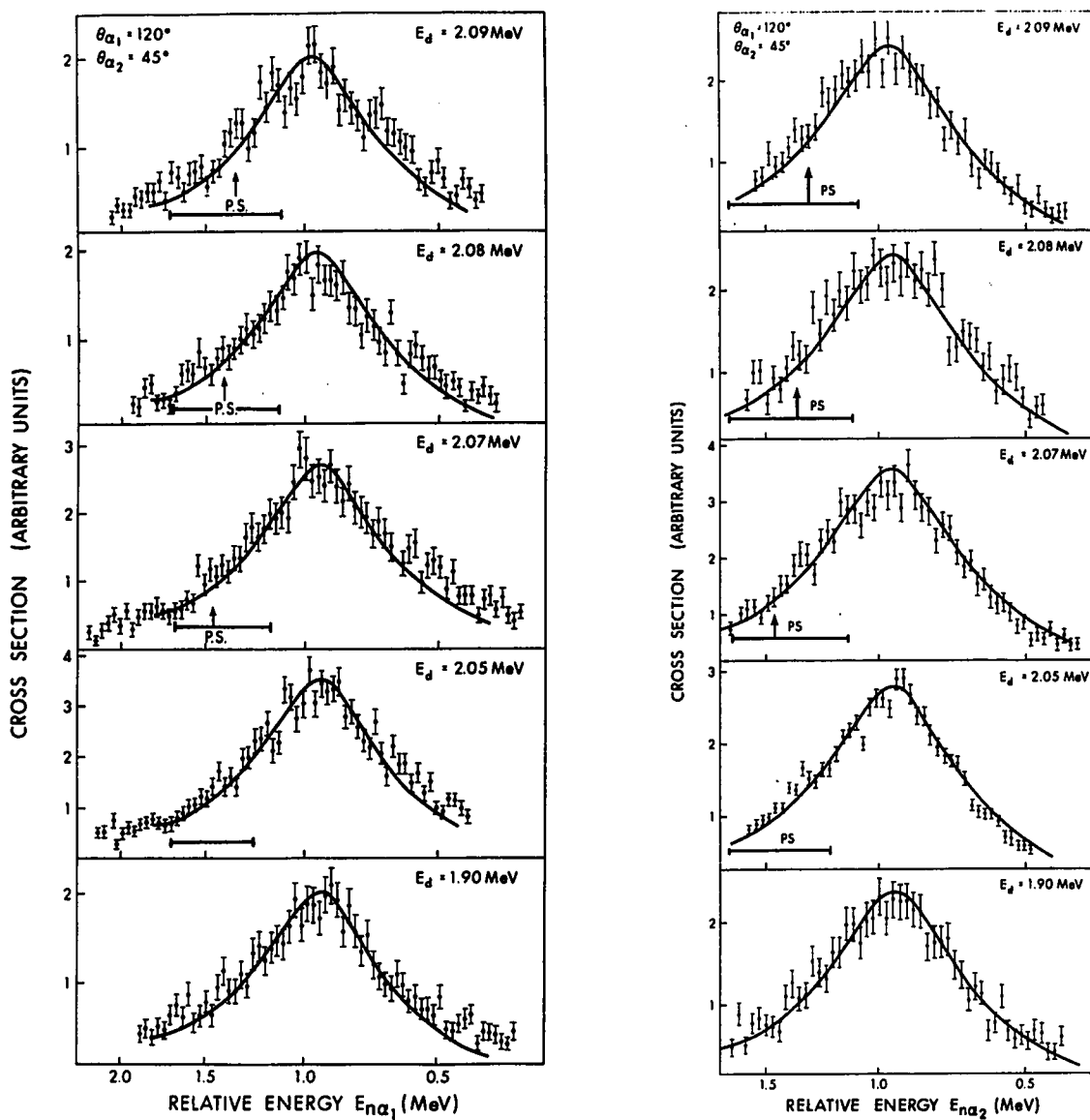
Figure 14   The data of figs. 12 and 13. The same Breit-Wigner resonance shape (plus linear background) has been fitted to the ^{5}He state in each case.

In order to search for rescattering effects at positions b and c in fig. 10, measurements were made at angles $\theta_{\alpha_1} = 115°$, $\theta_{\alpha_2} = 40°$ and an incident deuteron energy of 2.10 MeV. At these angles, the ^{9}Be (16.63 MeV) resonance is no longer kinematically allowed. Projections of events from this kinematic locus are shown in fig. 15, and again the positions where proximity scattering is allowed classically are shown.

d) Discussion

It is evident from figs. 8 and 12 that the effect in the previous data[13]) attributed to proximity scattering does not appear in the present measurements. There could be several reasons why one would not observe these effects.

The rapid variation of E_{resc} with incident beam energy, as shown in fig. 9, demands an accurate knowledge of both the incident beam energy and the spread in energy due to target thickness. These have, however, been carefully measured in the present case and should not appreciably smear out any effect.

Dispersion of the rescattering events due to finite angular acceptance could also be expected, but with acceptance of 1° in each detector a broadening of six channels for the data shown in fig. 12 is expected.

As discussed in section 4.1 (b) above, considerable smearing is to be expected due to the finite width of the 16.63 MeV state in ^{8}Be. The width of the 16.63 MeV state is 0.097 ± 0.011 MeV[45]). Fig. 9 shows that rescattering contributions must be expected over
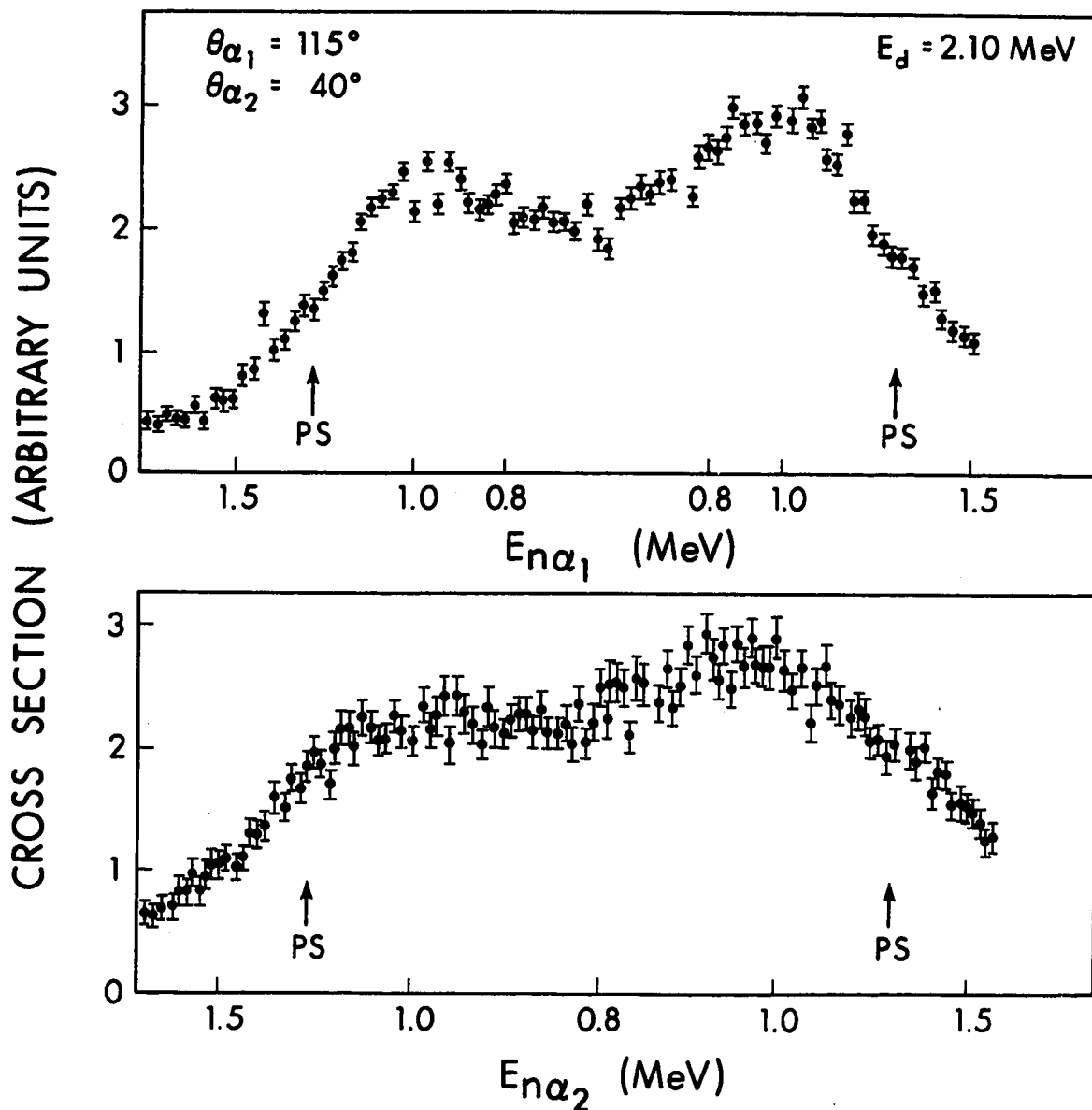
Figure 15 Data near the expected rescattering locations from regions c (upper) and b (lower) of fig. 9 at E_d = 2.10 MeV. The arrows mark the positions at which proximity scattering may occur. (Horizontal lines, as in figs. 8, 12 and 13, could have been drawn on this figure also.)

a range of $E_{n\alpha}$ relative energies of about 600 keV. This width is considerably greater than that of the enhancement shown in the data of Thiévent et al.[13]).

As mentioned in section 4.1 (b), separate runs were made to record "accidental" coincidence spectra, and appropriate subtractions were made. It is of some interest to note that accidental events are to be expected (with reference to fig. 10) both in horizontal and vertical "lines" due to "singles" rates from $^{16}O(d,p_1)^{17}O$ and $^{7}Li(d,\alpha)^{5}He$ respectively. The "crossover" of accidental coincidence lines shown near position d in fig. 10 also occurs very near to position a . In the latter case, the singles reactions are $^{16}O(d,\alpha_0)$ and $^{12}C(d,p_0)$ in the vertical direction and $^{7}Li(d,\alpha)^{5}He$ in the horizontal direction. Such lines were seen in the present experiment (along with others due to such reactions as $^{16}O(d,p_0)^{17}O$, $^{12}C(d,p_0)^{13}C$, etc.). Since these particular accidental lines cross in the vicinity of the ^{5}He and proximity scattering locations on the kinematic locus, their subtraction is clearly important. Thiévent et al.[13]) did not subtract accidental coincidences in spite of the reported presence of ^{16}O.

Sweeney et al.[15]) also repeated this experiment and have been unable to confirm the results reported by Thiévent et al.[13]).

4.2 The $^{12}C(d,n)^{13}N^*_{3.5}(p)^{12}C$ Reaction

a) Introduction

The first investigation of proximity scattering in the $^{12}C(d,np)^{12}C$ reaction was reported by Lang et al.[9]). They reported

the results of their measurements for one incident deuteron energy E_d = 5.39 MeV and angle settings θ_n = θ_p = 90°, ϕ_{np} = 0°, 10° and 30°. Another study of the $^{40}Ca(d,np)^{40}Ca$ reaction was reported by Lassen et al.[10]) at E_d = 5.8 MeV and for θ_n = θ_p = 70° and ϕ_{np} between 0° and 42.2°. These measurements appear to support the theoretical predictions of Aitchison and Kacser[4]).

Both experiments have been performed at only one bombarding energy. The observed enhancement may not necessarily be due to proximity scattering because one should note that the corresponding relative energy in the n-p system is very close to the energy of the T = 1 resonance in the neutron-proton system. It was suggested by Phillips[11,12]) that although the formation of this virtual deuteron resonance is isospin forbidden, an admixture of T = 0 state and T = 1 virtual states of the deuteron could, however, produce such an effect.

Figure 16 shows the two spectra for the $^{12}C(d,np)^{12}C$ reaction; one is measured by Lang et al.[9]) whereas the other is taken by Phillips[11,49]). The former shows the enhancement as an extended shoulder to the sequential peak, while in the latter case a sharp peak attributed to the n-p final state interaction occurs at 50 keV n-p relative energy. Hence, there is a strong contradiction in the shape of the measured energy spectra.

As no conclusive evidence of the observance of proximity scattering exists to date, the present search for the presence (or absence) of rescattering in the $^{12}C(d,np)^{12}C$ reaction was undertaken.
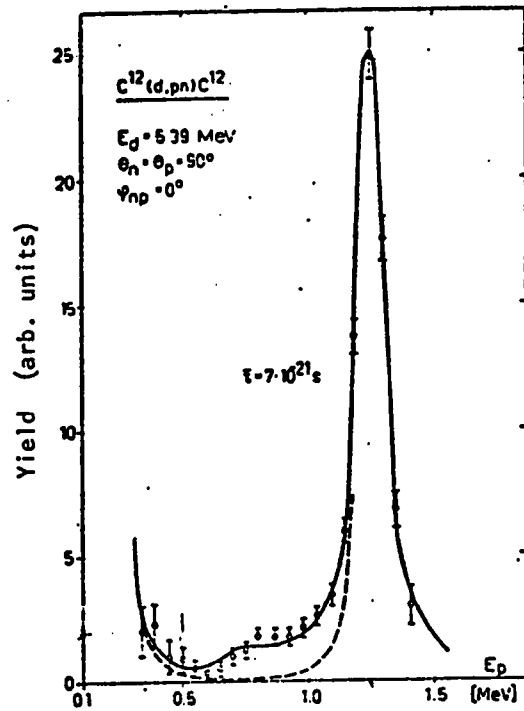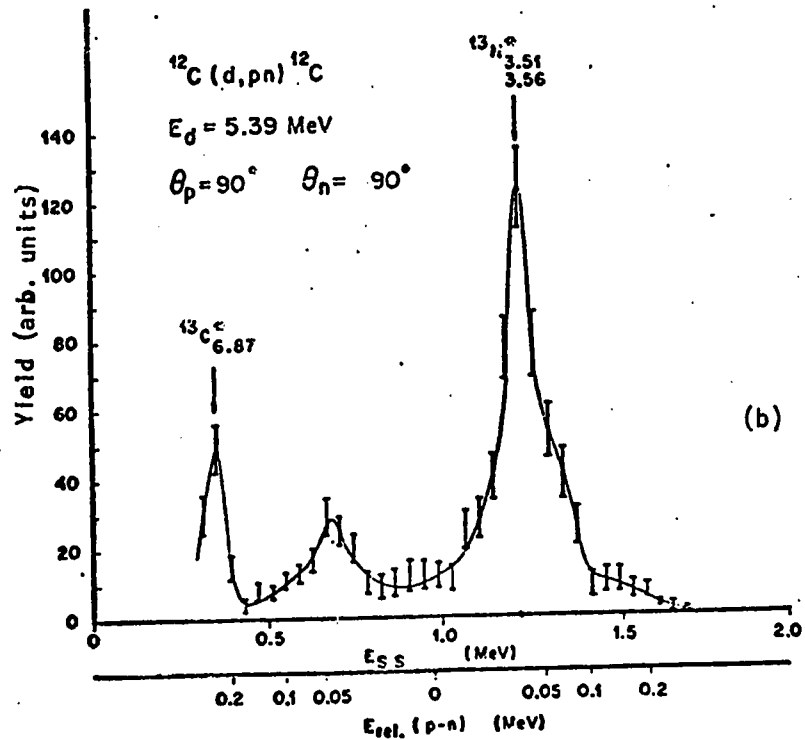
Figure 16   Comparison of data by a) Lang et al.[9]) and b) Phillips[11]); for the reaction $^{12}C(\overline{d,np})^{12}C$ at E_d = 5.39 MeV; θ_n = θ_p = 90°, ϕ_{np} = 0°.

Energy level diagrams for ^{13}C, ^{13}N and ^{14}N systems are shown in fig. 17. The doublet at 3.51 - 3.56 MeV excitation energies in ^{13}N decays by proton emission and is about 1.6 MeV above the threshold for decay (as this doublet can not be resolved in this experiment, it will be referred to as the 3.5 MeV level in further discussion). Therefore energy of emitted protons is above the threshold for experimental measurements. As this level is well separated from neighbouring levels, no interference from other levels is expected to contribute to the measured spectra. Also, the known widths of levels in this doublet ($\Gamma_{3.51} = 63 \pm 5$ keV; $\Gamma_{3.56} = 74$ keV[46]) are neither very large nor very small; they meet the criteria discussed in Chapter 2. These considerations along with the fact that the cross sections for the (d,n) reaction and the sequential decay process are large, make this reaction suitable for investigation of proximity scattering.

b) Experiment

Details of the (d,np) experiments have been discussed in Chapter 3 and an experimental set up is shown in fig. 5.

Data events were stored in a 128 x 128 channel array, one variable being the neutron time-of-flight, the other proton energy. The small background due to accidental coincidences has been subtracted channel by channel from the experimental data. To facilitate analysis of the data, events on the kinematic locus have been projected onto the proton energy axis.
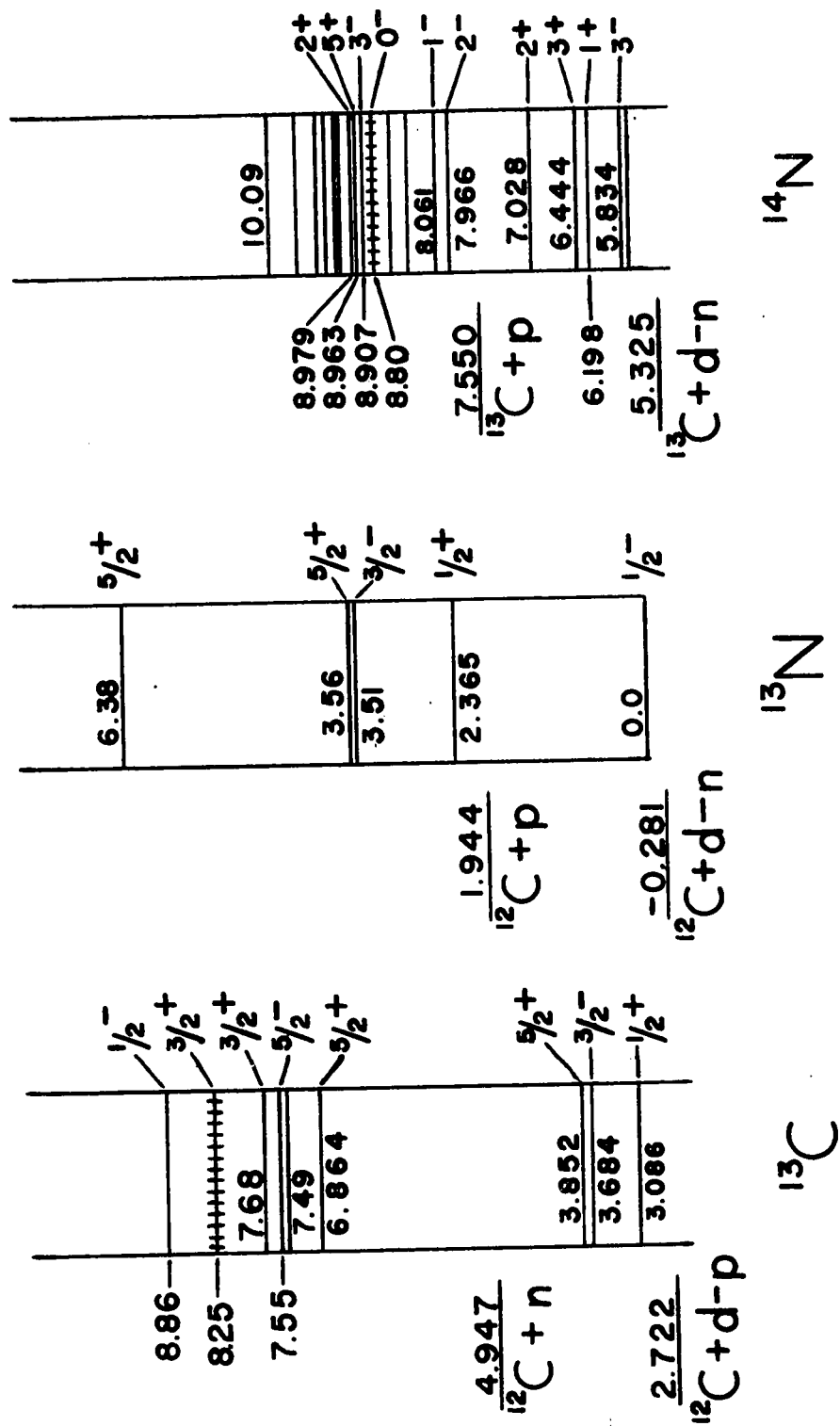
Figure 17   Level diagram of ^{13}C, ^{13}N and ^{14}N.

c) Results and discussion

   i) Energy dependence

   As discussed in Chapter 2 (eq. 2.41) the n-p rescattering energy E_{np}, is a function of the bombarding energy for a given reaction. Experimentally, an enhancement for a range of values of E_{np} is expected to be observed for a given bombarding energy, E_b. However, for a different incident energy $E'_b \neq E_b$, the range of relative energies of the n-p system changes. Thus, the only way to distinguish the rescattering effect from the contribution of known or unknown resonances is to observe a change in the relative energies at which the anomaly appears with a change in the bombarding energy. Fig. 18 shows the n-p relative energy in the rescattering process as a function of the deuteron bombarding energy.

   Data have been obtained at angular settings of $\theta_n = \theta_p = 90°$, $\phi_{np} = 0°$; and at the incident deuteron energies $E_d = 5.2$, 5.4, 5.75 and 6.25 MeV, respectively, and are shown in fig. 19. Typical error-bars are shown in each spectrum. As can be seen from the 5.2, 5.4 and 5.75 MeV data, the proximity scattering hump moves towards lower n-p relative energy, as we go up in bombarding energy. The relative energy is marked on a separate scale in this figure. The rescattering energy has been calculated in each case using eq. (2.41) and it corresponds to 74, 39 and 7 keV for 5.2, 5.4 and 5.75 MeV bombarding energies, respectively. Positions where the levels in $^{14}N^*$ and $^{13}C^*$ may contribute, are also marked by arrows. Their significance will be discussed later on.
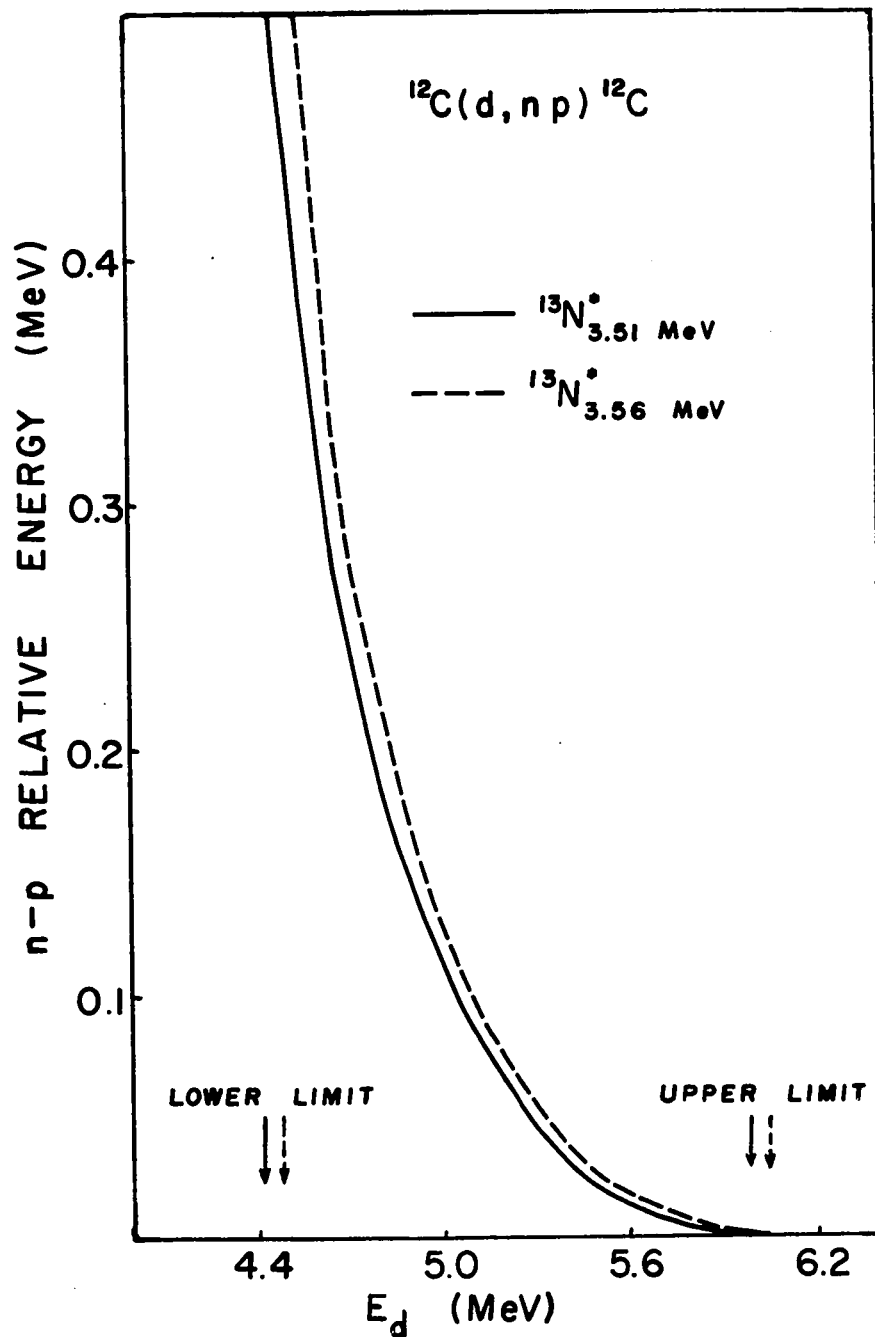
Figure 18   The variation of the n-p rescattering energy, E_{resc}, with incident deuteron energy, E_d for the reaction $^{12}C(d,np)^{12}C$. Solid and dashed curves correspond to the 3.51 and 3.56 MeV states of $^{13}N^*$ respectively. Arrows show the upper and the lower limits on E_d for the occurance of proximity scattering.
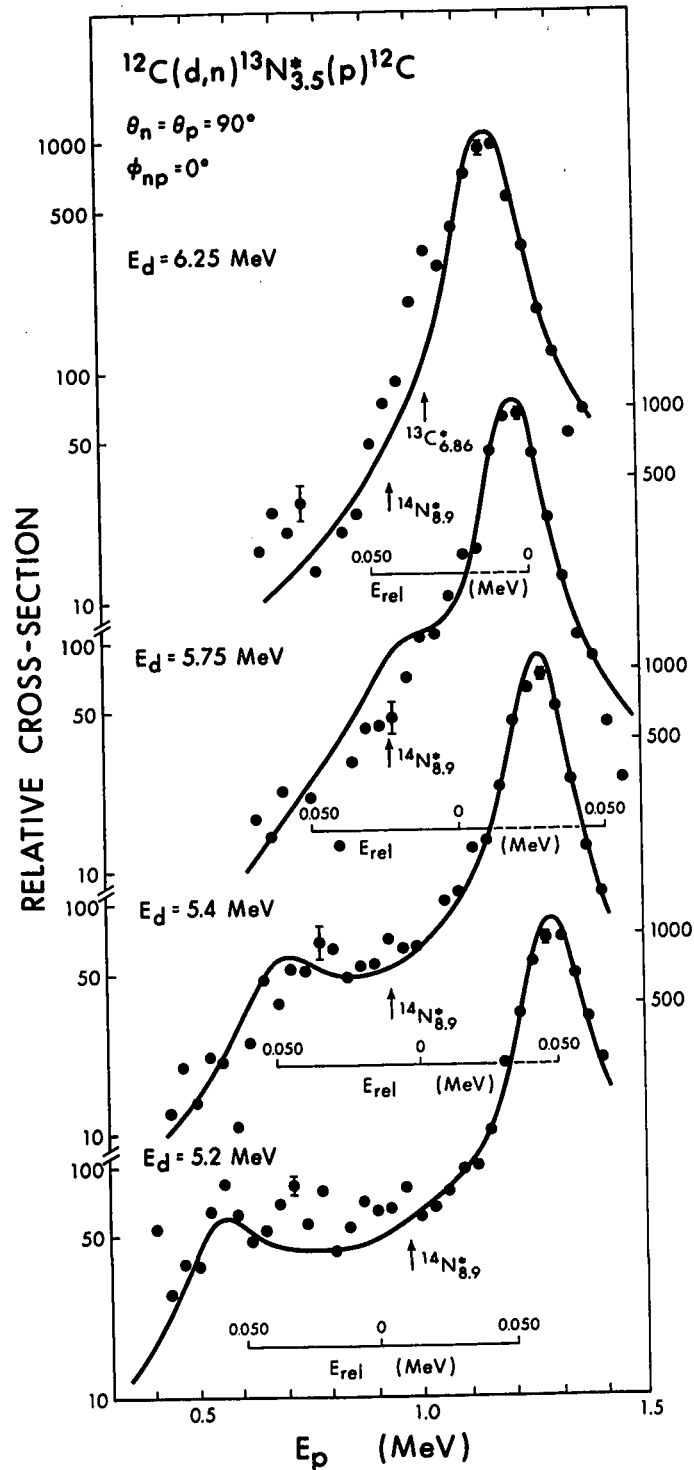
Figure 19 The present data for the $^{12}C(d,np)^{12}C$ reaction at E_d = 5.2, 5.4, 5.75 and 6.25 MeV; $\theta_n = \theta_p = 90°$, $\phi_{np} = 0°$, shown as projections onto the proton energy axis. Large peak is due to the sequential decay of $^{13}N^*$. Positions of sequential peaks due to $^{13}C^*$ and $^{14}N^*$ are shown by arrows. Solid curve is calculated from Aitchison and Kacser's[4] formalism of proximity scattering.

Another set of data has been obtained at E_d = 5.1, 5.26 and 5.4 MeV and at angular settings of θ_n = 78°, θ_p = 90° and ϕ_{np} = 0°, and is shown in fig. 20. Significance of these data will be brought out while discussing the effect of the n-p final state interaction. However, it may be pointed out that the proximity scattering enhancement, again, follows the proper energy dependence. Calculated values of the rescattering energy are 95, 62 and 39 keV, respectively, corresponding to bombarding deuteron energies of 5.1, 5.26 and 5.4 MeV.

The upper and lower limits on the bombarding energy for which the conditions of proximity scattering are met, can be calculated from eqs. (2.42) and (2.43) and are marked in fig. 18. For this reaction the upper limit is calculated to be 6.05 MeV, taking E_R as the centroid of the level in $^{13}N^*$; if the resonance energy is taken as E_R + $\Gamma/2$, E_b comes out to be ~6.1 MeV. In other words, above 6.1 MeV bombarding energy the proximity scattering is kinematically disallowed. To test this criteria, measurements were done at E_d = 6.25 MeV and angular settings of θ_n = θ_p = 90°, ϕ_{np} = 0°; and are also shown in fig. 19. There was no change in the experimental conditions during all four measurements shown in this figure. It is quite evident that these data agree with the predicted shape.

The curves shown by solid lines in fig. 19 (and in subsequent figures) have been obtained from the theoretical calculations using Aitchison and Kacser's formalism discussed in Chapter 2 (for
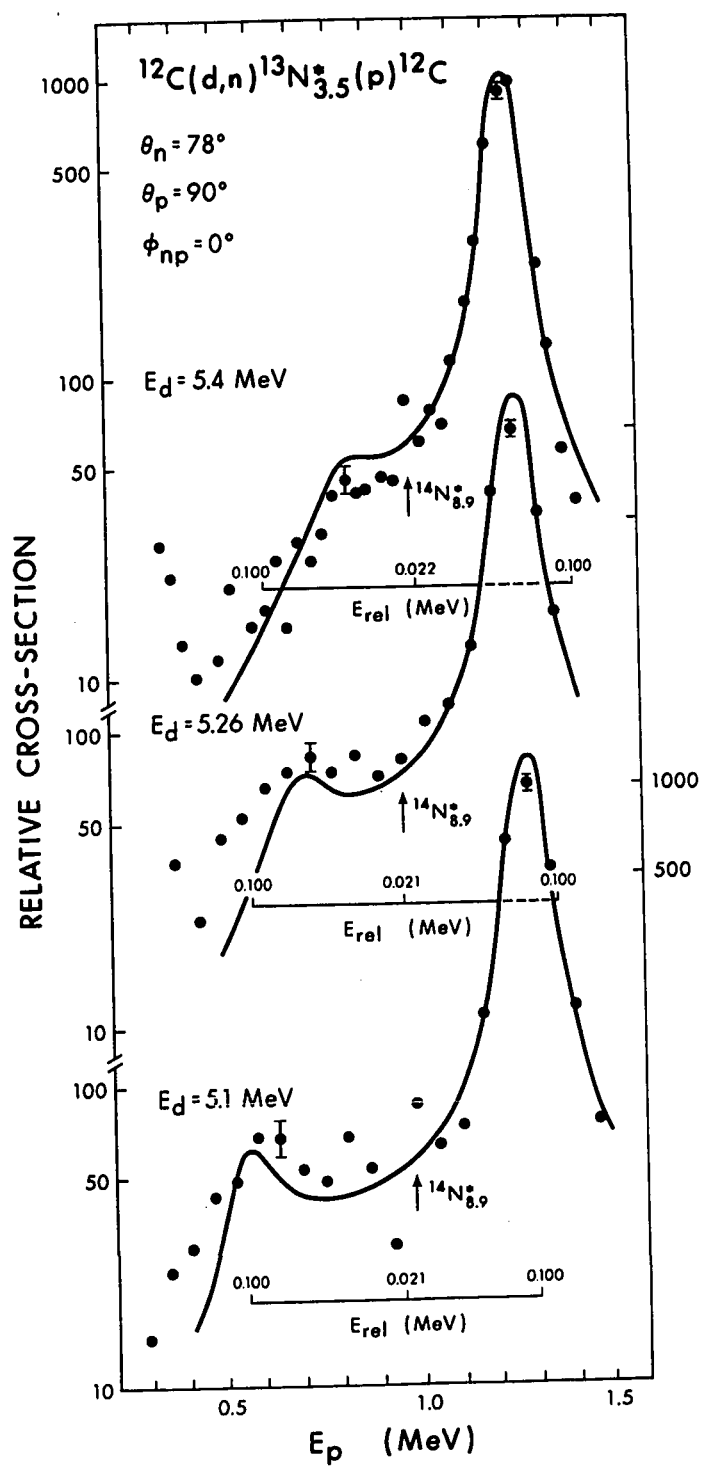
Figure 20 The present data for the $^{12}C(d,np)^{12}C$ reaction at $E_d = 5.1$, 5.26 and 5.4 MeV; $\theta_n = 78°$, $\theta_p = 90°$, $\phi_{np} = 0°$. The rest is the same as for fig. 19.

point geometry). The values of scattering parameters used in these calculations are given below[*7])

a_s (singlet scattering length) = - 23.7146 fm ,

a_t (triplet scattering length) = 5.43 fm ,

r_s (singlet effective range) = 2.76 fm , and

r_t (triplet effective range) = 1.70 fm .

As stated in Chapter 2 (eq. 2.52), Γ is the only variable quantity in the expression for the cross section. The line shape of the sequential peak in the present data seems to fit well with the predicted shape, if Γ = 80 keV is used as the width of the 3.5 MeV doublet in ^{13}N.

ii) Azimuthal angular dependence

If the n-p relative energy, E_{np}, is plotted versus $E_{p-^{12}C}$, the relative energy in p-^{12}C system, for E_d = 5.4 MeV and $\theta_n = \theta_p$ = 90°, ϕ_{np} = 0°, 10°, 20°, 30°; the diagram will look like a series of Dalitz plots, one each for a value of ϕ_{np}. Aitchison[8]) in his talk at the Brela Conference showed that the enhancement due to proximity scattering is maximum at ϕ_{np} = 0°, i.e., when both the detectors are in the same plane. For higher values of ϕ_{np}, this enhancement decreases. At ϕ_{np} = 30°, the proximity scattering bump should disappear (because E_{np} is above the shaded band in fig. 2b). A measurement performed at $\theta_n = \theta_p$ = 90°, ϕ_{np} = 35° and at an incident deuteron energy E_d = 5.4 MeV is shown in fig. 21. For the sake of comparison the data for ϕ_{np} = 0° are also shown. One can see that the results of these
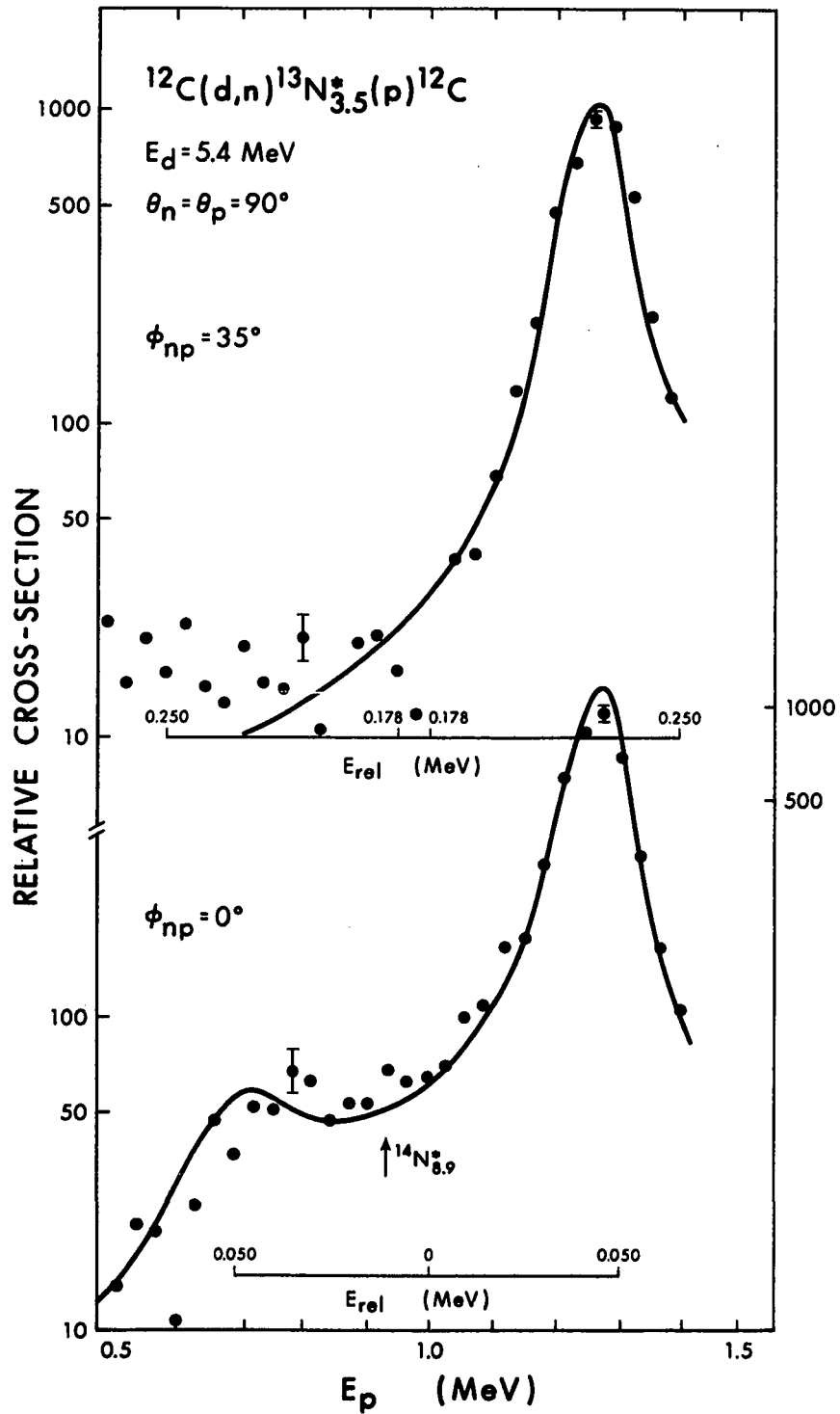
Figure 21   Comparison of the data at E_d = 5.4 MeV; θ_n = θ_p = 90° for ϕ_{np} = 0° and 35°.

measurements are in good agreement with the theoretical predictions.

iii) Contribution from other resonances

A level at 2.38 MeV excitation in $^{13}N^*$ can also decay by proton emission. It is, however, expected to give a peak at $E_p \simeq 0.25$ MeV and thus, does not interfere with the present results. The protons emitted from this level have lower energy than that of the previously emitted neutrons and hence, do not satisfy the conditions of proximity scattering.

The reaction can also proceed as: $^{12}C(d,p)^{13}C^*(n)^{12}C$. From the energy level diagram for ^{13}C shown in fig. 16, one can see that the 6.86 MeV level can contribute to the measured spectra. From figs. 18 and 19 it is evident that the only spectrum where it gives its contribution is the one taken at $E_d = 6.25$ MeV. In all other cases the peak due to this process lies at very low proton energies. This peak in the 6.25 MeV data is also not very significant.

Natural carbon which contains about 1% of ^{13}C was used for making the targets. Fig. 17 shows that a number of levels at about 8.9 MeV excitation energy in ^{14}N lie in the region corresponding to 3.5 MeV excitation in ^{13}N. These levels in $^{14}N^*$ also can decay by proton emission via the reaction $^{13}C(d,n)^{14}N^*(p)^{13}C$. The regions where events from the $^{13}C(d,np)^{13}C$ reaction occur have been marked in figs. 19 to 21. In order to assess the contribution due to this reaction, separate runs were taken using self-supporting thin ^{13}C targets, under conditions similar to the ^{12}C runs.

The measured spectra for the ^{13}C + d reaction taken at $E_d =$

5.4 and 6.25 MeV and angular settings $\theta_n = \theta_p = 90°$, $\phi_{np} = 0°$, are shown in fig. 22. These data were normalized to a unit charge of the incident beam and their contribution to the ^{12}C + d spectra was determined. The amount of ^{13}C in the ^{12}C target was determined by taking singles spectra for the ^{13}C(d,p)^{14}C reaction and obtaining counts for the same peak in the two measurements; ^{13}C contamination was verified to be ~1%. The factor f by which the counts in spectra shown in fig. 22 should be divided to estimate the ^{13}C contribution to the measured proximity scattering spectra is given by:

$$f = \frac{\text{charge for } ^{13}\text{C run}}{\text{charge for } ^{12}\text{C run}} \times 100$$

and resulted in the values of f = 7.3, 15.5 for the bombarding energies E_d = 5.4 and 6.25 MeV, respectively. Thus, one can see from fig. 22 and figs. 19 to 21 that the contribution due to ^{13}C contamination is insignificant.

iv) Role of n-p final state interactions

As stated in section 4.2 (a), n-p f.s.i. could also give an enhancement at low n-p relative energies. Experimental evidence regarding violation of isospin selection rules can be divided into two categories.

Class one deals with positive evidence for isospin forbidden peaks. Von Witsch et al.[48]) studied the d + d → d + p + n reaction at E_d = 11, 12 and 13 MeV. Their data contained a strong peak in
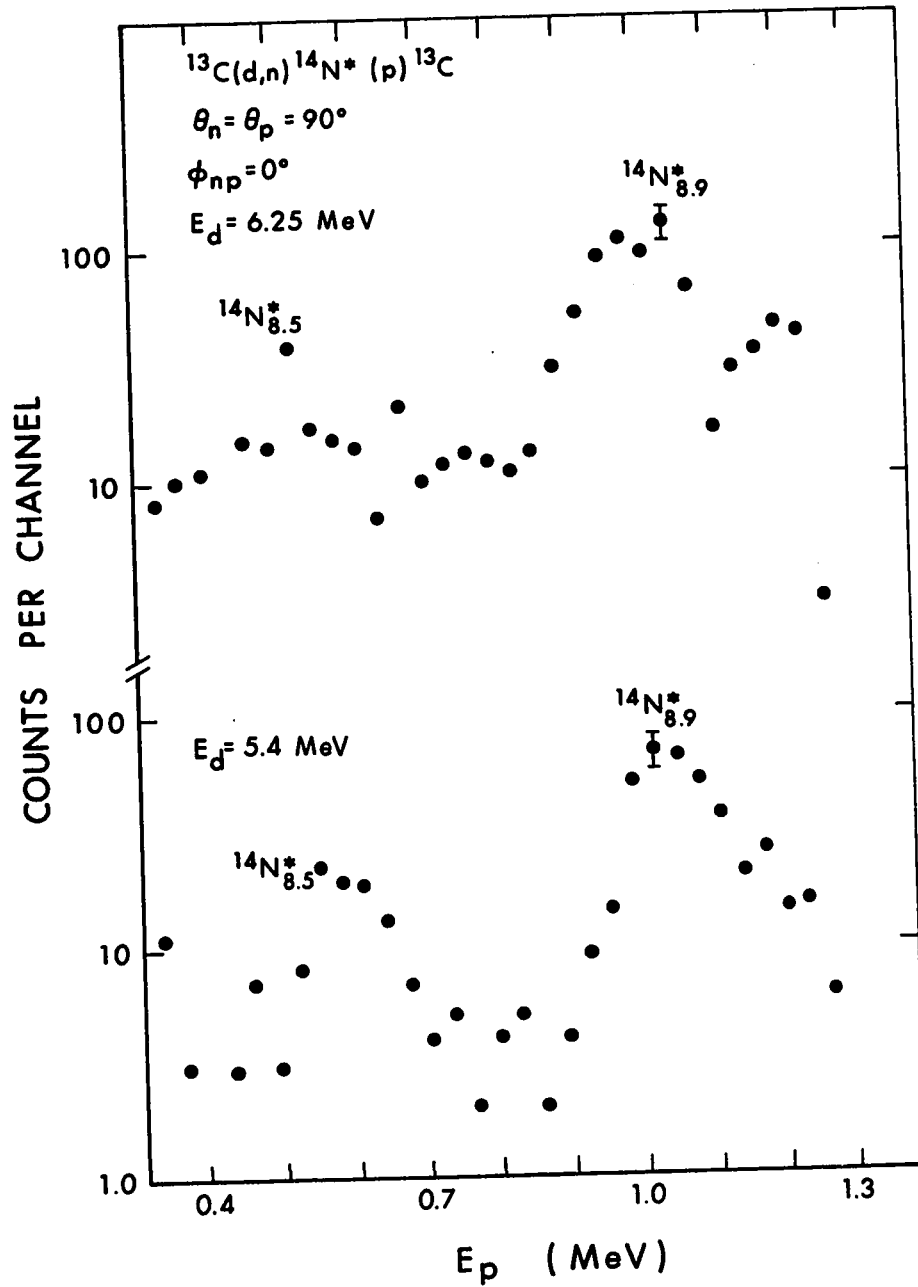
Figure 22   The present results for the $^{13}C(d,np)^{13}C$ reaction at E_d = 5.4 and 6.25 MeV; θ_n = θ_p = 90°, ϕ_{np} = 0°.

the kinematic region near $E_{pn} = 0$, which was difficult to explain. However, they interpreted their results by taking this peak as evidence for some of the p-n system being formed in the isospin-forbidden "singlet deuteron" state. Calculations based on this assumption did not give good fits to the data, but required a singlet:triplet mixing in the ratio 1:2 to qualitatively reproduce the observed enhancement.

In another study reported by Smith et al.[50], similar isospin mixing in the compound system ^{14}N has been used to explain the large cross section for the $^{12}C(d,\alpha)^{10}B$ (1.74 MeV, T = 1) reaction which is also isospin forbidden.

The second category of experiments where no evidence of isospin mixing has been found is mentioned below. A study of the reaction $d + \alpha \rightarrow {^4He} + p + n$ done at $E_\alpha = 24$ MeV by Assimakopoulos et al.[51] has shown no evidence of singlet-triplet mixing in the p-n final state. Good theoretical fits to the data were obtained by assuming a pure triplet interaction and an upper limit of 3% was placed on the possible singlet admixture.

Measurements made by von Witsch et al.[52] of the reaction $^6Li + d \rightarrow {^6Li}_{g.s.} + p + n$ at $E_d = 10$ MeV show no evidence for isospin mixing. No qualitative upper limit could be set due to the presence of other f.s.i.'s in the same kinematic region. They further suggested that the effects observed in ref. 48 might not be due to the isospin-forbidden $^1S_0$ p-n interaction, but are possibly due to some interference effects. In a rather conclusive

study on the ^{6}Li(d,pn)^{6}Li reaction performed at E_d = 21 MeV by Braithwaite et al.[53]), it has been shown that there is a complete isospin separation of the p-n interaction. The strong p-n final state enhancement observed near E_{pn} = 0 had isospin T = 1 when the reaction proceeded through the 3.56 MeV (T = 1) state of the residual nucleus, ^{6}Li. An upper limit of 2% was placed on the $^1s_0$ (T = 1) contribution to the triplet spectra (for ^{6}Li$_{g.s.}$ and ^{6}Li$_{2.18}$, both T = 0) and an upper limit of 10% was placed on the $^3s_1$ (T = 0) contribution to the singlet spectra.

Thus on the existing evidence, one cannot catagorically reject sequential decay through a T = 1 deuteron virtual state as an explanation for the enhancement in the present data, although it would seem very improbable. Hence an effort was made to clearly distinguish the role of p-n final state interactions from proximity scattering, in present measurements.

The first step taken to achieve the above objective was to select a suitable angular setting so that E_{np} = 0 does not lie on the kinematic locus. In order to be able to detect the rescattering effect in the lab. system, one has to choose a pair of angles such that there is at least one point on the E_p versus E_n plot (kinematic locus) which corresponds to the excitation energy of E_{np} in the intermediate n-p system. Or looking at the Dalitz plot (fig. 2 (b)), the choice of the angles should be such that the boundary of the Dalitz plot should cross the rescattering band. This condition was satisfied with the angular setting θ_n = 78°,

θ_p = 90°, ϕ_{np} = 0°. The lowest n-p relative energy possible with this setting was ~21 keV for bombarding energies between 5.1 and 5.4 MeV. Whereas, proximity scattering amplitude remains unchanged with this choice of angles, the Watson-Migdal prediction shows a reduction by a third in the amplitude for n-p final state interactions (maximum enhancement occurs at E_{np} = 0). Measured data for E_d = 5.4 MeV and angular settings θ_n = 78°, θ_p = 90°, ϕ_{np} = 0° and θ_n = θ_p = 90°, ϕ_{np} = 0° are shown in fig. 23. No apparent change in the proximity scattering amplitude is noticeable. Fig. 20 shows the energy dependence of rescattering at above angles; this further strengthens the argument that an insignificant role is played by p-n final state interactions. Another advantage of choosing an unequal pair of angles is to eliminate any possible absorption of low energy neutrons in the solid state detector and its mount, because it no longer obstructs the neutron detector.

As a second step taken to identify the n-p final state interaction contribution in the present measurements, the 5.4 MeV data were fitted with the Briet-Wigner line shape plus a mixture of the singlet and triplet states of the deuteron. A Monte-Carlo routine was used to simulate the Briet-Wigner shape for the sequential peak as well as to calculate the singlet and triplet shapes for n-p interaction. Computed values for the triplet were fitted with a function T;
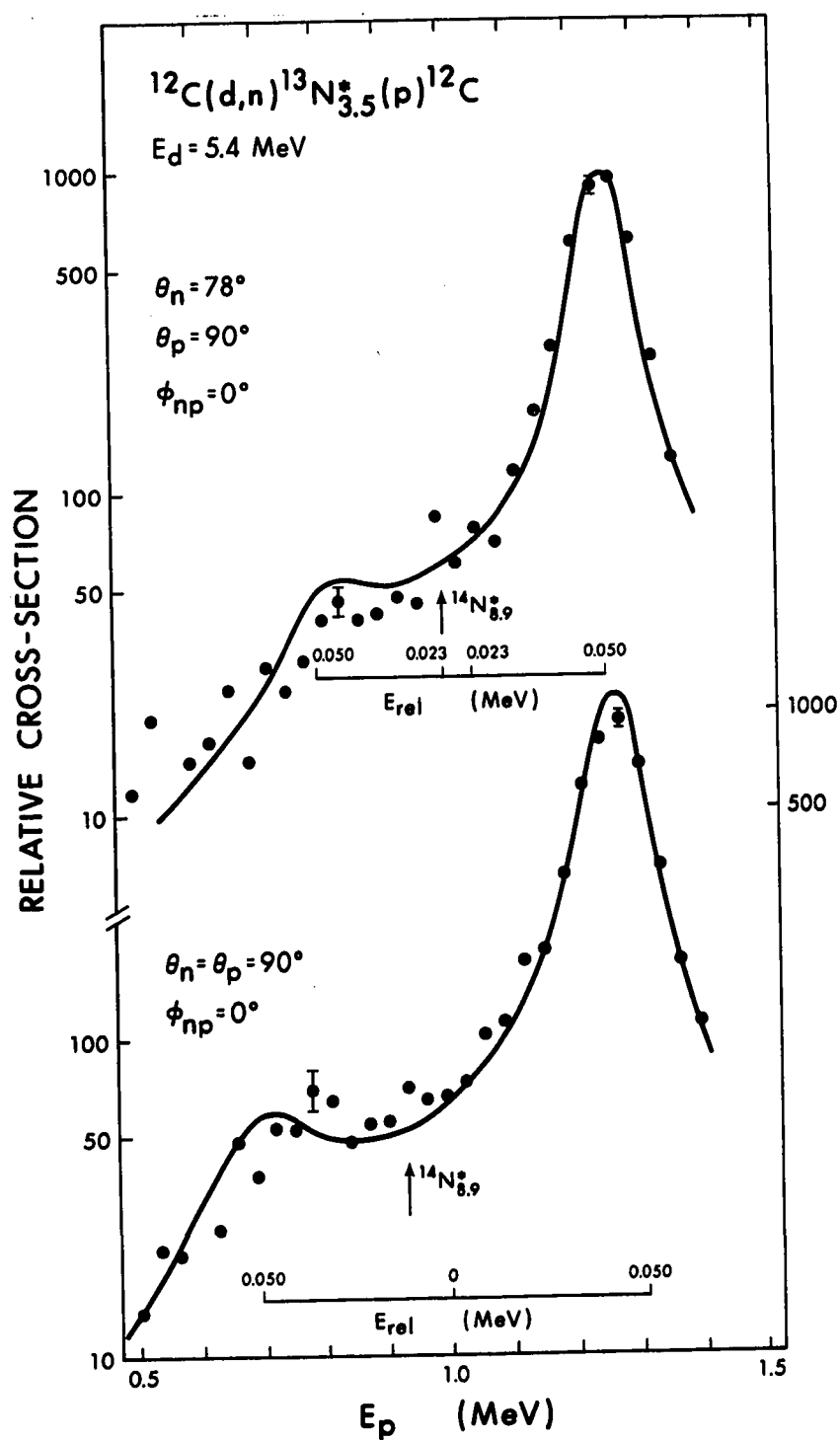
$$T = a + bx + cx^2 + dx^3 ,$$

Figure 23 Comparison of the data at E_d = 5.4 MeV for angle settings θ_n = θ_p = 90°, ϕ_{np} = 0° and θ_n = 78°, θ_p = 90°, ϕ_{np} = 0°.

while the singlet was fitted with a function S;

$$S = a' + b'x + c'x^2 + d' \left(\frac{e'^2}{(x-g)^2 + \frac{1}{4} e'^2} \right)$$

Best values of the coefficients a, b, c, d and a', b', c', d', e' and g were found using a χ^2 program on the SDS-920 computer.

Finally, the experimental data were fitted with a function, FUNCT;

$$FUNCT = AT + BS + \left(\frac{CE^2}{(x-G)^2 + \frac{1}{4} E^2} \right)$$

and the best values of the coefficients A, B, C, E and G were determined. This fit is shown in fig. 24 and represents a <3% singlet contribution relative to the triplet.

As can be seen, the data do not agree very well with such a calculation. This further confirms the belief that proximity scattering exists in this reaction.

4.3 The $^{28}Si(d,n)^{29}P^*_{4.34}(p)^{28}Si$ Reaction

This reaction was also studied as part of the present research. The measurements were performed at bombarding energies $E_d = 4.9$ to 5.7 MeV and angular settings $\theta_n = \theta_p = 60°$, $\phi_{np} = 0°$, 30°; $\theta_n = 48°$, $\theta_p = 60°$, $\phi_{np} = 0°$. Levels at 3.45 and 4.08 excitation energies in $^{29}P^*$ can also decay by proton emission and their sequential peaks appear in the same region where proximity scattering due to the 4.34 MeV level is expected to occur. Also, ^{12}C contamination was found in all the five targets which were tried.
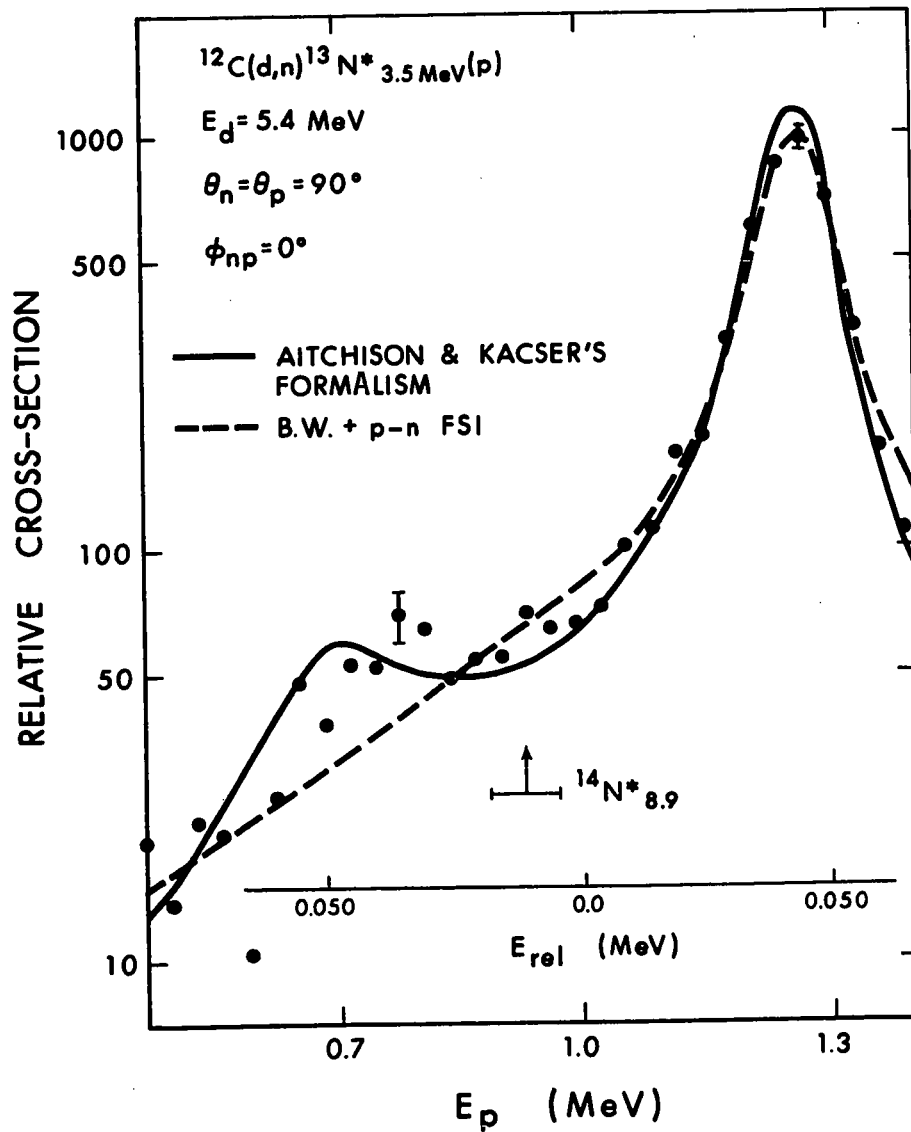
Figure 24   Breit-Wigner plus n-p final state interactions fit
(shown as dashed curve) to the data at E_d = 5.4
MeV; θ_n = θ_p = 90°, ϕ_{np} = 0°. The solid curve
represents the proximity scattering prediction of
Aitchison and Kacser[4]).

The sequential peak due to ^{12}C contamination shows up quite strongly very near to the sequential peak due to ^{29}P$^*_{4.34}$. Thus the presence of these interfering sequential decays made it quite difficult to extract any meaningful contribution due to proximity scattering.

CHAPTER 5

TRIANGLE SINGULARITIES IN ELEMENTARY PARTICLE PHYSICS

A brief discussion of rescattering effects in elementary particle physics is appropriate here. A typical reaction is

$$\pi + N \to \pi + R \to \pi + \pi + N$$
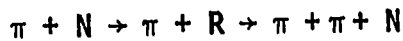
with R corresponding to the N* spin-$\frac{3}{2}$ πN resonance. Aitchison[16]) has shown that there is a logrithmic singularity in the amplitude of this reaction. He assumed that in the process $\pi + N \to \pi + N^*$, the initial state is $D_{\frac{3}{2}}$, which implies S-state production of the N*. The N* $\to \pi N$ breakup is P-wave and the $\pi\pi$ rescattering is then a pure S-wave.

This process can be represented by a triangle graph shown in fig. 1(e), where b and t refer to π and N, 1' and R correspond to π and N* the (3,3) nucleon isobar, 2' and 3 refer to π and N, and 1 and 2 are both π's. N* is taken as a spinless particle of complex mass. In ref. 16, this graph is calculated from a dispersion relation as a function of the mass s of the two pions in the final state for low values of the overall C.M. system energy W . The relation is then analytically continued in W . For a narrow range in W , an enhancement of the square of the amplitude is found near s = 4 (the pion mass is 1, two pion mass is $\sqrt{s}$). The analog-

ous enhancement also appears in the W channel near $W = R + 1$, for a small range of s only, near $s = 4$. The prominence of the effect depends on the width of R, being closely connected with the nearness to the physical region of one of the two logarithmic singularities (anamolous thresholds) of the graph: this distance increases sharply with the isobar width. The positions of singularities are interpreted as the phase-space limits for the simultaneous production of states with mass s and R . Aitchison concluded that such a "double excitation" process leads to an enhancement of the triangle amplitude only if, in general, s and R fall in certain narrow ranges. In summary, the effect if observable, should show up as a bump in the production process if two pions are observed near threshold $(s = 4)$. This is unfortunate because the detection of this may prove difficult.

Good examples of triangle singularities are hard to come by in elementary particle physics. This is one reason why it was suggested by Aitchison to look for this effect in low energy nuclear physics. However, the work of Anisovich and Dakhno[54] is a reasonably good example in which they explain the anomalous behaviour of the pion-pion mass distribution at $s = 4$ ($M_{\pi\pi} \sim 2$) in the reactions $\pi^- + p \rightarrow n + \pi^+ + \pi^-$ and $p + d \rightarrow {}^3He + 2\pi$, by means of triangle singularities. The reaction $\pi^- + p \rightarrow n + \pi^+ + \pi^-$ was experimentally investigated by Kirz et al.[55] at incident pion energy $E_\pi = 360$ to 780 MeV. Their data clearly show a bump at $E_\pi = 360$, which

gradually disappears with the increase in incident energy. Abashian et al.'s[56] experimental data for the reaction $p + d \rightarrow {}^{3}He + 2\pi$ show that the increase of the double pion production probability near the region $s \sim 4$ disappears at $E_p \geq 1300$ MeV.

CHAPTER 6

CONCLUSIONS

The $^7Li + d \rightarrow n + \alpha + \alpha$ reaction was investigated to verify the positive evidence for n-α rescattering reported by Thiévent et al.[13] The measurements were performed at E_d = 1.90 to 2.10 MeV. The data do not show any enhancement due to Proximity Scattering. Strong accidental lines due to the "singles" rates from the reactions $^{16}O(d,p)^{17}O$, $^{16}O(d,\alpha)^{14}N$, $^{12}C(d,p)^{13}C$ and $^7Li(d,\alpha)^5He$ were seen in the vicinity of the positions on the kinematic locus where rescattering occurs. The enhancement reported in ref. 13 may have been due to these random coincidences. The data, after proper subtraction due to r a n d oms, are fitted well with a Breit-Wigner line shape plus linear background using Monte Carlo simulation. This does not necessarily imply the non-existence of proximity scattering. At these low energies, this effect must be expected to be greatly smeared out by the width of the intermediate $^8Be(16.63)$ MeV state. Experiments performed at higher energies where the effect is more localized have, however, also failed to show rescattering contribution[12].

In the data for the $^{12}C(d,np)^{12}C$ reaction, the energy dependence of the proximity scattering is clearly illustrated at E_d = 5.1 to 5.75 MeV (figs. 19 and 20). The data for E_d = 6.25 MeV (fig. 19) do not show any enhancement; this is in accordance with the

theoretical predictions because at E_d > 6.1 MeV the proximity

scattering is kinematically disallowed. At the azimuthal angle

ϕ_{np} > 30°, no contribution due to proximity scattering is expected;

this is supported by the data for E_d = 5.4 MeV and angle setting θ_n =

θ_p = 90°, ϕ_{np} = 35° (fig. 21). Finally, possible contributions due to

the singlet and triplet states of the deuteron are found to be quite

small. The 5.4 MeV data have been fitted with the Breit-Wigner line

shape plus a mixture of n-p final state interactions in the $^1s_0$ and

$^3s_1$ states. One can see from fig. 24 that the fit is not very good.

.Thus, in conclusion, the present measurements on the $^{12}C(d,np)^{12}C$

reaction strongly support the existence of proximity scattering and

serve to reject alternative explanations of the previous results

(refs.[11,12]).

REFERENCES

1) R. Fox, Phys. Rev. 125 (1962) 311

2) H.J. Schnitzer, Rev. Mod. Phys. 37 (1965) 666

3) I. Duck, Nucl. Phys. 57 (1964) 643

4) C. Kacser and I.J.R. Aitchison, Phys. Rev. 142 (1966) 1104 and Phys. Rev. 152 (1966) 1518

5) C. Kacser and I.J.R. Aitchison, Rev. Mod. Phys. 37 (1965) 350

6) I.J.R. Aitchison, Nuovo Cim. 35 (1965) 434

7) C. Kacser, Phys. Lett. 12 (1964) 269

8) I.J.R. Aitchison, Few Body Problems - Proc. Brela Conf., Ed: Paic and Slaus (1967) p. 607

9) J. Lang, R. Müller, W. Wölfli, R. Bösch and P. Marmier, Nucl. Phys. 88 (1966) 576 and Phys. Lett. 15 (1965) 248

10) L. Lassen, W. Zahradnik and B. Zeitnitz, Nucl. Phys. A120 (1968) 645 and Phys. Lett. 24B (1967) 338

11) G.C. Phillips, Proc. Intern. Conf. on Clustering Phenomenon in Nuclei, Bochum (1969)

12) V. Valković, C. Joseph, A. Niiler and G.C. Phillips, Nucl. Phys. A116 (1968) 497

13) G. Thiévent, J. Lang, R. Müller and P. Marmier, Phys. Lett. 30B (1969) 23 and Nucl. Phys. A170 (1971) 17

14) K.H. Bray, J.M. Cameron, G.C. Neilson and T.C. Sharma, Nucl. Phys. A181 (1972) 319

15) W.E. Sweeney, Jr., V. Valković, D. Rendić and G.C. Phillips, Phys. Lett. 37B (1971) 183

16) I.J.R. Aitchison and C. Kacser, Phys. Rev., 133 (1964) B1239 and also I.J.R. Aitchison, Phys. Rev. 133 (1964) B1257

17) L. Schiff, Quantum Mechanics (McGraw-Hill Book Co., Inc., New York, 1955) p. 199

18) E. Ferrari and F. Selleri, Nuovo Cim., Suppl. 24 (1962) 453

19) M.L. Goldberger and K.M. Watson, Collision Theory (John Wiley and Sons, Inc., New York, 1964) Chapter II.

20) I.E. McCarthy, Introduction to Nuclear Theory, (John Wiley and Sons, Inc., New York, 1968) p. 480

21) C. Werntz, Phys. Rev. 128 (1962) 128

22) H.W. Lefevre, R.R. Borchers and C.H. Poppe, Phys. Rev. 128 (1962) 1328

23) (a) Proceedings of the Conference on Correlations of Particles Emitted in Nuclear Reactions, held at Gatlinburgh, Tennessee, Oct. 1964; Rev. Mod. Phys. 37, No. 3, (1965)

    (b) Proceedings of the International Nuclear Physics Conference, held at Gatlinburgh, Tennessee, Sept. 1966 (Academic Press, New York, 1967) Session IX

    (c) Proceedings of First International Conference on the Three Body Problem in Nuclear and Particle Physics, held at Birmingham, July 1969 (North-Holland Publ. Co., Amsterdam, 1970)

24) A.B. Migdal, JETP 1 (1955) 2

25) M. Veltman, CERN Report (64-13)

26) M.L. Goldberger and K.M. Watson, ibid, p. 479

27) S. de Benedetti, Nuclear Interactions (John Wiley and Sons, Inc., New York, 1964) p. 159

28) K.M. Watson, Phys. Rev. 88 (1952) 1163

29) J. Gillespie, _Final State Interactions_ (Holden-Day, Inc., San Francisco, 1964) p. 2

30) J. Gillespie, ibid, Chapter 2

31) E. Fermi, _Elementary Particles_ (Yale University Press, New Haven, Conn. 1951) p. 58 -64

32) J. Gillespie, ibid, Chapter 3

33) C. Zupancic, Rev. Mod. Phys. $\underline{37}$ (1965) 332

34) R.J.N. Phillips, Nucl. Phys., $\underline{53}$ (1964) 650

35) J.D. Jackson and J.M. Blatt, Rev. Mod. Phys. $\underline{22}$ (1950) 77

36) J. Gillespie, ibid, Chapter 4

37) R. Jost and W. Kohn, Phys. Rev. $\underline{82}$ (1951) 840

38) G.C. Phillips, T.A. Griffy and L.C. Biedenharn, Nucl. Phys. $\underline{21}$ (1960) 327

39) I.S. Sherman, R.G. Roddick and A.J. Metz, IEEE Trans. $\underline{NS-15}$ (1968) 500

40) A.H. Hussein, M.Sc. Thesis, University of Alberta (1970) unpublished

41) W.W. Lindstrom and B.D. Anderson, Nucl. Instr. and Meth. $\underline{98}$ (1972) 413

42) F.T. Kuchnir and F.J. Lynch, IEEE Trans. Nucl. Sci. $\underline{NS-15}$ (3) (1968) 107

43) D.A. Gedcke and W.J. McDonald, Nucl. Instr. and Meth. $\underline{55}$ (1967) 377 and $\underline{58}$ (1968) 253

44) G.C. Neilson, J.D. Panar and L. Holm, Nucl. Instr. and Meth. $\underline{76}$ (1969) 75

45) T. Lauritsen and F. Ajzenberg-Selove, Nucl. Phys. $\underline{78}$ (1966) 1

46) F. Ajzenberg-Selove, Nucl. Phys. A$\underline{152}$ (1970) 30

47) E.H. Henley, Isospin in Nuclear Physics (John Wiley and Sons, Inc., New York, 1969) p. 15

48) W. von Witsch, M. Ivanovich, D. Rendic, J. Sandler and G.C. Phillips, Phys. Rev. C2 (1970) 2144

49) J. Sandler, V.A. Otte and G.C. Phillips, Bull. Am. Phys. Soc. 15 (1970) 471

50) H.V. Smith and H.T. Richards, Phys. Rev. Lett. 23 (1969) 1409

51) P.A. Assimakopoulous, E. Beardsworth, D.P. Boyd and P.F. Donovan, Nucl. Phys. A144 (1970) 272

52) W. von Witsch, W. Ivanovich, V.A. Otte, D. Rendic and G.C. Phillips, Nucl. Phys. A172 (1971) 633

53) W.J. Braithwaite, J.M. Cameron, J.G. Cramer, C.R. Rudy and W.W. Eidson, Phys. Lett. 38B (1972) 67

54) V.V. Anisovich and L.D. Dakhno, Phys. Lett. 10 (1964) 221

55) J. Kirz, J. Schwartz and R.D. Tripp, Phys. Rev. 130 (1963) 2481

56) A. Abashian, N. Booth and K. Crowe, Phys. Rev. Lett. 5 (1960) 258 and Phys. Rev. Lett. 7 (1961) 35

57) J.M. Cameron, G.C. Neilson and T.C. Sharma, Proc. Int. Conf. on Few Particle Problems in Nucl. Phys., held on Aug. 28 - Sept. 1, 1972, at UCLA, U.S.A. (to be published)

58) T.C. Sharma, J.M. Cameron and G.C. Neilson, Nucl. Phys. (to be published

59) H. Gemmeke, D. Baumgartner, A. Richter and L. Lassen, Proc. Int. Conf. on Few Particle Problems in Nucl. Phys., held on Aug. 28 - Sept. 1, 1972, at UCLA, U.S.A. (to be published)